Deepwater channel-lobe transition zone dynamics: processes and depositional architecture, an example from the Karoo Basin, South Africa

Hannah L. Brooks [1]*, David M. Hodgson [1], Rufus L. Brunt [2], Jeff Peakall [1], Menno Hofstra[1], Stephen S. Flint [2]

[1] Stratigraphy Group, School of Earth and Environment, University of Leeds, Leeds, UK, LS2 9JT

[2] Stratigraphy Group, School of Earth and Environmental Sciences, University of Manchester, Manchester, M13 9PL, UK.

Corresponding author: eehlb@leeds.ac.uk

Journal GSA Bulletin

Key words: Channel-lobe transition zone (CLTZ); bypass; base of slope; stepped slope profile; Karoo Basin.

ABSTRACT

Submarine channel-lobe transition zones (CLTZs) form morphologically complicated areas, commonly located at breaks-in-slope, and separate well-defined channels from well-defined lobes. These areas play a vital role in the transfer of sediment through deepwater systems. Extensive outcrop exposures in the Karoo Basin, South Africa, permit investigation of the depositional architecture and evolution of entirely exhumed dip transects of a CLTZ for the first time. Furthermore, the excellent paleogeographic constraint allows correlation to genetically related updip channel-levee systems and downdip lobe deposits over 40 km, with strike control over 20 km. Unlike the single time slice afforded by modern systems, the Karoo example uniquely allows study of the temporal shifting of the CLTZ and transfer into the stratigraphic record.

Key lateral changes along the base of slope include the variation from an inter-fingering levee to lobe transition zone to a bypass dominated CLTZ over a width of 14 km. Key recognition criteria for CLTZs in the ancient record include combinations of scours and megaflutes, composite erosional surfaces, mudstone clast/coarse-grained sediment lags, and remnants of depositional bedforms, such as sediment waves. Documented here in a single CLTZ, these features are arranged in a zone of juxtaposed remnant erosional and depositional features. The zone reaches 6 km in length, formed by at least four stages of expansion/contraction or migration. Strike variations and changes in the dimensions of the CLTZ through time are interpreted to be the result of physiographic changes and variations in flow dynamics across the base of slope. The dynamic nature of CLTZs results in complicated and composite stratigraphy, with preservation potential generally low but increasing distally and laterally from the mouth of the feeder channel system. Here, we present the first generic model to account for dynamic CLTZ development, encompassing distinctive recognition criteria, fluctuations in the morphology and position of the zone, and the complex transfer into the sedimentary record.

INTRODUCTION

Deepwater channel-lobe transition zones (CLTZs) separate well-defined channels from well-defined lobes, and are areas within turbidite systems where sediment gravity flows undergo rapid expansion due to abrupt decrease in confinement and/or gradient change (Mutti and Normark, 1987; 1991). The understanding of CLTZ formation and dynamics is therefore pertinent in discerning and predicting facies distributions and the depositional architecture of submarine fans. Studies of systems on the present-day seabed, hereafter referred to as 'modern', show that CLTZs comprise a distinctive assemblage of erosional bedforms including isolated and coalesced scours, and depositional bedforms including sediment waves and lag deposits (e.g. Kenyon and Millington, 1995; Kenyon et al., 1995; Palanques et al., 1995; Wynn et al., 2002a; Fildani and Normark, 2004). CLTZs are dominated by sediment bypass processes, with a relatively thin record of erosion and deposition (Mutti and Normark, 1987; 1991; Normark and Piper, 1991; Stevenson et al., 2015; Covault et al., 2017). Models of CLTZs developed from modern seabed studies convey the distribution of erosional and depositional bedforms at a point in time (e.g. Kenyon et al., 1995; Palanques et al., 1995; Wynn et al., 2002a, 2002b; Dorrell et al., 2016), with potential to look at short periods via repeat surveys (e.g., Hughes Clarke et al., 2012), but do not allow the capture of long term (hundreds to thousands of years) changes in the dimensions and character of CLTZs. To do this requires stratigraphic control.

CLTZs have not been reported in detail from subsurface systems. As modern seabed examples show they are common features, this is likely due to the limited vertical resolution (typically 10-20 m) of reflection seismic data. However, several exhumed sections of CLTZs have been interpreted (e.g. Mutti and Normark, 1987; Vicente Bravo and Robles, 1995; Ito, 2008; van der Merwe et al., 2014; Hofstra et al., 2015; Pemberton et al., 2016; Postma et al., 2016). Within the stratigraphic record CLTZs are recorded either as a single surface separating lobes and channel fills (e.g. Elliott, 2000; Gardner et al., 2003) or expressed as a net depositional rock volume (e.g. Hofstra et al., 2015; Pemberton et al., 2016) displaying similar scour features shown in modern seabed datasets. However, limitations in paleogeographic constraint, and dip and strike control on depositional architecture have precluded the development of more advanced evolutionary models. As CLTZs are dominated by erosion and sediment bypass processes their preservation in the rock record requires them to later aggrade (e.g. Pemberton et al., 2016) or for feeder channels to be abandoned or to avulse before they cannibalize the zone (e.g. Hofstra et al., 2015). Furthermore, sediment bypass criteria, which may be used to recognize ancient CLTZs, have been synthesised from a wide range of systems and settings (e.g. Stevenson et al., 2015), but never constrained from an entire exhumed sediment bypass dominated zone.

Here, we present four sub-parallel dip-oriented >20 km long correlation panels from continuous outcrops, that capture the transition downdip from slope to basin-floor deposits in Units D/E and E of the Permian Fort Brown Formation, Karoo Basin, South Africa. These data are used to understand the dynamic evolution of a base of slope environment, including a uniquely well-exposed CLTZ, within subunit E3, with excellent paleogeographic constraint to genetically related up- and downdip deposits. Specific objectives are: i) to identify recognition criteria for a CLTZ in the ancient record; ii) to constrain the three-dimensional depositional architecture of an exhumed CLTZ; iii) to examine the spatial extent and temporal changes of a CLTZ; and iv) to discuss the transfer of CLTZs into the stratigraphic record and to present the first dynamic model of their evolution.

TERMINOLOGY

Here, we use the definition of Mutti and Normark (1987, 1991) and Wynn et al. (2002a) for CLTZs as ‘the region that, within any turbidite system, separates well-defined channels or channel-fill from well-defined lobes or lobe facies’, and thus CLTZs form in sand-detached geographic areas (*sensu* Mutti, 1985). CLTZs are examples of sediment bypass-dominated zones (*sensu* Stevenson et al., 2015).

GEOLOGICAL BACKGROUND AND LOCATION OF STUDY

The Karoo Basin has been traditionally interpreted as a retroarc foreland basin (Visser and Prackelt, 1996; Visser, 1997; Catuneanu et al., 1998). More recent studies (Tankard et al., 2009, 2012) suggest that subsidence during the deepwater phase of the basin was controlled by mantle flow over a complex arrangement of basement blocks. The late Carboniferous to Jurassic Karoo Supergroup comprises approximately 8000 m of sediments divided into the Dwyka, Ecca and Beaufort Groups (Fig. 1). The Permian Ecca Group in the Laingsburg depocenter records the eastward progradation of the basin margin with a stratigraphic succession from basin-floor deposits (Vischkuil and Laingsburg formations; van der Merwe et al., 2010) through channelized submarine slope (Fort Brown Formation; Hodgson et al., 2011; Di Celma et al., 2011) to shelf-edge and shelf deltas (Waterford Formation; Jones et al., 2015) (Fig. 2). Units C-F of the Fort Brown Formation have been mapped in detail over 2500 km^2 from slope valleys, downdip through channel-levee systems, to basin-floor lobe complexes (van der Merwe et al., 2014), and are separated by regional mudstone (claystone and siltstone) units (Fig. 2).

The Fort Brown Formation comprises Units B/C, C, D, D/E, E, F and G respectively (Fig. 2) and regional studies have led to the interpretation of each unit as a lowstand sequence set (Flint et al., 2011). This study focuses on Units D/E and E (Fig. 2B), which are exposed along a series of sub-parallel post-depositional fold limbs (Fig. 3). Detailed mapping and correlation of Unit E in this study utilizes regional correlation work undertaken in previous studies in this area (Figueiredo et al., 2010, 2013; Flint et al., 2011; van der Merwe et al., 2014; Spychala et al., 2015). Unit E comprises three depositional sequences, each including a sand-rich lowstand systems tract (LST; subunits E1, E2, and E3) and a related transgressive/highstand systems tract mudstone, which is approximately 1-8 m thick between each LST (Figueiredo et al., 2010, 2013).

Regional mapping and correlation of Units C to F have demonstrated an architectural change from sand-attached (Units C and D) to sand-detached CLTZs (Units E and F) (*sensu* Mutti, 1985; van der Merwe et al., 2014). The recognition of intraslope lobes in Units D/E and E (Fig. 4) (Figueiredo et al., 2010; Spychala et al., 2015), which are also known as perched lobes (Plink-Björklund and Steel, 2002; Prather et al., 2012) and transient fans (Adeogba et al., 2005; Gamberi and Rovere, 2011), supports the presence of a stepped slope profile at the time of deposition (van der Merwe et al., 2014; Fig. 4). This paper focuses on the sedimentology and stratigraphic expression of Unit D/E and subunits E2 and E3, over an area with channel-levee systems mapped updip and lobe complexes downdip, supporting deposition on the lower slope to basin-floor (van der Merwe et al., 2014). This also characterizes the sediment bypass-dominated zone recognized in subunit E3 (van der Merwe et al., 2014), as a CLTZ.

METHODOLOGY

Collection of over two hundred measured sections permitted construction of four sub-parallel >20 km long correlation panels oriented along depositional dip (Fig. 3), with this area of interest between channel-levee and lobe systems, recognized from previous regional studies (van der Merwe et al., 2014; Fig. 4). Logged sections document the lithology, grain size, sedimentary structures and stratal boundaries at cm scale resolution. The correlation framework was established by walking stratigraphic surfaces between sections and using regional mudstones (Fig. 4; van der Merwe et al. 2014). The top of underlying sand-rich Unit D is used as a datum as it is a basin-floor fan over the study area (van der Merwe et al., 2014; Hodgson et al., 2016) with minor thickness changes healed partially by the D-E mudstone. Structurally restored paleocurrent data were collected from ripple laminations, flutes and grooves. Spatial data are presented in palinspastically restored positions according to calculated post-depositional south to north shortening of 17.2% (Spikings et al., 2015). The Slagtersfontein detailed panel was constructed by closely spaced logged sections, with photopanels and detailed sketches aiding interpretation of erosional and depositional bedforms.

FACIES GROUPS

Eight distinct groups of lithofacies are described and interpreted in terms of sedimentary processes (Table 1; Fig. 5).

ARCHITECTURAL ELEMENTS

The stratigraphic context of Units D/E and E has been well established (Figueiredo et al., 2010; Flint et al., 2011; van der Merwe et al., 2014; Spychala et al., 2015). Five broad environments of deposition are identified based on the occurrence of constituent facies and facies groups, mapped geometries, paleogeographic context, and utilizing the depositional environment interpretations of previous studies in the Fort Brown Formation (Hodgson, 2009; Prélat et al., 2009; Hodgson et al., 2011; Kane and Hodgson, 2011; Brunt et al., 2013a, 2013b; Morris et al., 2014; Spychala et al., 2015):

1) External levees (Piper and Deptuck, 1997 Deptuck et al., 2007; Kane et al., 2007; Kane and Hodgson 2011; Morris et al., 2014): These deposits are dominated by thin-bedded

siltstone and sandstone, and structured sandstone, with high proportions of current ripple and climbing ripple laminated beds with consistent paleocurrent directions (Fig. 5F). Locally, chaotic deposits form where levees have collapsed. External levees have been mapped for up to 10 km away from their genetically-related channels, which are not identified within this study. Downdip, packages can be laterally continuous for several kilometers and change in thickness and facies. Typically, successions fine- and thin-upwards due to decreasing overspill during levee construction (e.g., Hiscott et al., 1997; Peakall et al., 2000; Kane and Hodgson, 2011). The tabular geometry, lateral continuity and consistent paleocurrent direction, characterize these successions as external levees (cf. Kane and Hodgson, 2011).

2) Lobe deposits: Lobes are subdivided into transitional sub-environments, lobe axis, lobe off-axis and lobe fringe, based on decreasing sand content and decreasing degree of bed amalgamation (Prélat et al., 2009; Prélat and Hodgson, 2013). Lobe axis deposits primarily comprise thick-bedded, amalgamated structureless sandstone (Fig. 5A), and represent deposition of high-energy sediment-laden turbidity currents. Lobe off-axis deposits comprise stratified successions of medium-bedded, structured sandstones with more tractional structures (Fig. 5B) formed by deposition from comparatively lower energy currents. Lobe fringe deposits comprise thin-bedded, sandstone and siltstone (Figs. 5E, 5F), deposited from dilute currents and/or silt-rich hybrid beds, resulting from entrainment of fine-grained sediment and mudstone clasts (Ito, 2008; Haughton et al., 2003, 2009; Baas et al., 2011) . At kilometer-scale this architectural element is lobate in planform and lens shaped in cross-section (e.g. Prélat et al., 2009, 2010).

3) Sediment bypass-dominated zones (van der Merwe et al., 2014; Stevenson et al., 2015): These are characterized by thin deposits of discontinuous structureless and structured sandstone beds (Fig. 5B) commonly highly dewatered due to rapid deposition (Lowe, 1988). Composite erosion surfaces and scours (< 2 m deep) are draped by cm to 10's of cm lag deposits of coarser grained material (medium-grained sandstone and mudstone clasts (Fig. 5C)), but without major (more than several meters) incision. The large scale geometry of this architectural element is thin (10 cm – 5 m) and highly discontinuous (varying over 10's of meter downdip).

4) Spill-over fringes: These tabular, thin-bedded siltstone deposits are extensive over the study area and represent a subdivision of the interbedded sandstone and siltstone facies

(type iii). Their distinctive tabular geometry and lateral continuity and monotonous facies over 10’s of kilometers distinguishes these deposits from lobe fringes which can be traced laterally over kilometer scale to genetically related sand-rich lobe deposits. The stratigraphic and geographic position of this facies, downdip of intraslope lobes, supports an interpretation that it represents flows that partially breached updip confining topography, causing the flow to be stripped as the fine-grained, upper, low-density portion of flows continued downdip (into the study area) (Piper and Normark, 1983; Sinclair and Tomasso, 2002). Coarser grained portions of flows are ponded updip in intraslope accommodation, as demonstrated by Spychala et al. (2015). This facies is similar in appearance to lobe fringe deposits, but is spatially disconnected from its genetically-related lobe axis deposits.

5) Regional mudstone (siltstone and claystone) drapes (Fig. 5H): These 3-50 m thick units are extensive and laterally continuous (10s to 100 km) hemipelagic mudstones, present between all units and subunits, aiding correlation.

CORRELATION PANELS

The four sub-parallel correlation panels (Figs. 6 and 7) permit 2D sedimentological and stratigraphic analysis, and help constrain the 3D depositional architecture of the system (Fig. 8). Overall, paleocurrent trends throughout the study area are towards the east (Figs. 6 and 9); therefore panels are oriented broadly parallel to paleoflow.

Unit D/E

Unit D/E is a discontinuous unit, up to 12 m thick and present within the regional D-E mudstone which varies in thickness (10-50 m) (Fig. 6). Throughout the study area, Unit D/E has a sharp base and top, and paleocurrents towards the E/ENE (Fig. 9A). In the north of the study area (panel 1; Figs. 7A, 8 and 9A), the unit consists of a single <1 m thick debrite. In the central area (panel 2; Figs. 7B, 7C, 8 and 9A), Unit D/E is discontinuous around Slagtersfontein, and then thickens south (panel 3) and east from a few cm to 12 m, transitioning from lobe fringe and off-axis to lobe axis. In an intervening area along panel 3 (Figs. 7C, 8 and 9), the Unit abruptly thins and fines to <1 m of siltstone. In this interval, and where Unit D/E thins and pinches out eastward it is associated with numerous clastic injectites (cf. Cobain et al., 2015) (Figs. 7B, 7C and 8). Unit D/E also thins and fines abruptly southward (panel 4; Figs. 7D, 8 and 9A).

The sharp base and top, with no evidence of erosion, indicate abrupt initiation and cessation of sand supply. The comparatively abrupt southward transition over 3 km from sandstone through thin-bedded siltstone to pinch out (Fig. 9A) suggests topographic confinement (Smith, 2004a; Spychala et al., 2017). The northward transition is more gradual (Fig. 9A) and is interpreted as unconfined. The facies distribution, elongate geometry and paleogeographic context are consistent with weakly confined lobes that intercalate with subtle (< 1°) topography (Smith, 2004a; Spychala et al., 2017). The abrupt changes in thickness suggest deposition over irregular seabed topography. The location of the feeder channel is poorly constrained due to exposure limitations but is interpreted to be out of the study area towards the southwest based on the paleocurrent and thickness trends (Fig. 9A).

Subunit E1

The pinch out of E1 (Fig. 2) occurs updip to the west of the study area (Figueiredo et al., 2010), and does not feature as part of this work.

Subunit E2

In the north (panel 1; Figs. 6A and 7A), E2 comprises 0.5-1 m of spill-over fringe deposits overlain by 2-3 m of external levee deposits for 14 km downdip. Over the following 2 km downdip, the unit thickens to 5-6 m, with localized contorted strata (Figs. 6A, 7A and 8). Downdip, E2 pinches out or is incised by E3. In the updip part of panel 2 (Figs. 6B and 7B), E2 similarly comprises spill-over fringe deposits overlain by external levee deposits. Downdip in the Slagtersfontein area, E2 coarsens and consists of structured and structureless sandstone, which thicken and thin abruptly (0-3 m) over meter-scale distances due to basal scouring and onlap on to underlying topography, and is overlain by thin (<15 cm) silt-rich hybrid beds, interpreted as lobe fringe deposits (Figs. 7B, 8 and 9). Two kilometers farther downdip, in an area where the underlying D-E mudstone is thinner (Figs. 6B, 7B, 8 and 9), E2 abruptly fines to thin-bedded, spill-over fringe deposits. Continuing downdip, E2 thins from 5 to 1 m and maintains this thickness for a further 12 kilometers until it thins or is eroded out in the east. In the most updip 4 kilometers of the southerly panels (Fig. 6C, 7C and 7D), E2 comprises a single 1-2 m bed of structureless sandstone with rip-up clasts, that abruptly pinches out downdip, with numerous associated clastic injectites.

The external levee deposits in the northwest of the study area (Figs. 7A, 7B and 8) are likely related to confined channels in the subcrop to the north (Fig. 9B). The deposits at Slagtersfontein (panel 2), and to the south (panels 3 and 4), are interpreted as lobe fringes. The abrupt sand-prone pinch outs of E2 in the south (Figs. 6C, 7C and 7D) follow a similar pattern to the underlying Unit D/E suggesting topographic confinement (Fig. 9B). The sand-prone pinch out and observed basal scouring and thickness changes in the Slagtersfontein study area are discussed further in the detailed section below (Figs. 10 and 11).

Subunit E3

A thin package (<0.5 m) of spill-over fringe deposits is present at the base of E3 where there is limited overlying erosion. In the north this package is overlain by external levee deposits (2-5 m thick) for 14 km downdip. These transition in to 2-3 m of thin-bedded and silt-rich hybrid bed, lobe fringe deposits, and medium-bedded structured and structureless sandstone lobe off-axis deposits. E3 then abruptly thickens into 20 m of thickly-bedded sand-rich lobe axis and off-axis deposits and maintains a similar thickness and facies downdip (Figs. 6A, 7A, 8 and 9C).

The most updip 4 kilometers of E3 in panel 2 (Figs. 6B and 7B) consists of external levee facies that thin basinward from 10 to 4 m. Downdip at Slagtersfontein (Figs. 3, 6B and 7B), the external levee is truncated by a composite erosion surface overlain by bypass-dominated facies. Further downdip, E3 thickens abruptly (20 cm to >4 m) over 40 m, and for a further 700 m downdip comprises 1-5 m of lobe axis sandstone with a scoured base and top and common internal soft-sediment deformation. Here, the base of E3 cuts down several meters through the E2-E3 intra-unit mudstone, and locally removes E2 over outcrop lengths of meters to 10s of meters (Figs. 6B, 7B and 9C). The top surface of E3 is cut by a bypass assemblage of 1-3 m long scours, mantled by mudstone clasts and/or draped with thin siltstone beds. Farther downdip, E3 thickens abruptly to 19 m over 200 m (a rate of 9 cm/m), and is dominated by lobe axis deposits and sand-rich hybrid beds. Two hundred meters farther downdip the unit reaches 40 m thick, with truncation of basal beds (Fig. 7B). E3 remains 37-39 m thick, and then thins to 18 m over 1 kilometer with thick axial lobe deposits and few hybrid beds (Figs. 7B and 9C). E3 continues to thicken and thin (between 16 and 37 m) farther basinward, with an overall transition from lobe axis to lobe off-axis and lobe fringe deposits (Figs. 6B, 7B, 8 and 9C).

Across strike to the south (panels 3 and 4; Figs. 6C, 7C and 7D) updip E3 comprises 22-35 m of thick-bedded amalgamated lobe axis sandstones with a sharp base and top to the unit. Locally, a scoured top surface is marked by >10 m long and >4 m wide megaflutes with superimposed ripple lamination (Figs. 6C and 7C). Downdip, beyond 7 kilometers of no exposure, E3 thins from 15 to 6.5 m over 1 kilometer, comprising lobe off-axis sandstones and silt-rich hybrid bed prone lobe fringe deposits. Here, the top surface is scoured, with erosion surfaces mantled by mudstone clasts. Downdip of this area, the upper part of E3 is not preserved due to present day fluvial erosion. Thicknesses are therefore minimum values (Figs. 6C and 7C). For 11.5 kilometers, E3 is at least 7-14 m thick, comprising lobe off-axis and fringe deposits, with localized contorted, chaotic and disaggregated bedding (Figs. 7C and 8). For the remaining 3.5 kilometers of exposure, E3 thickens to 37 m, dominated by lobe axis amalgamated sandstone (Figs. 7C and 8) with minor off-axis and fringe deposits. In the far south (panel 4), after initial thick axial deposits, E3 thins to 4 m over 9 kilometers downdip (Figs. 7D, 8 and 9) followed by an abrupt change to chaotic deposits and lobe fringe siltstone for 18 kilometers. Distally, deposits thicken and coarsen abruptly into 15 m of lobe off-axis, lobe axis and minor thin-bedded fringe material (Figs. 7D, 8 and 9).

External levee deposits in the northwest of the study area likely confine channels in the subcrop. The sediment bypass-dominated zone is restricted to the Slagtersfontein study area (Figs. 7B, 8 and 9) with a minor component in updip panels 3 and 4. Slagtersfontein is discussed in more detail below (Figs. 10, 11 and 12). In the south, the thinning and pinch out of E3 downdip suggests a similar pattern of intrabasinal confinement recognized in the underlying units D/E and E2 (Figs. 8 and 9) indicating the presence of a broadly north-facing intrabasinal slope. Lobe fringe deposits are silt-rich hybrid bed prone lateral to the interpreted lobe axis (panel 1, proximal lobe deposits, panel 3, downdip of an area of no exposure). In more distal areas these become more thin-bed dominated (eastern areas of panels 2, 3, and 4).

SLAGTERSFONTEIN DETAILED SECTION

The sedimentology and depositional architecture of subunits E2 and E3 are considered in more detail in the Slagtersfontein area as they change abruptly in facies and character downdip. The Slagtersfontein area is split into 5 sections (Section 1 updip to Section 5 downdip) for description purposes (Figs. 10, 11 and 12), which are supported by closely spaced logged sections measured at mm resolution (Fig. 13). The near-continuous presence of the underlying E2 and the E2-E3 mudstone in this area (Figs. 10 and 11) suggests there are no deep scour- or channel-fills of E3 age.

Section 1

Subunit E2 comprises spill-over fringe (0.5 m) overlain by external levee deposits (<3 m). E3 comprises similar facies with thicker external levee deposits (<5 m) overlain by a thin-bedded siltstone package (up to 0.5 m) containing subtle erosion surfaces and thin (cm-scale) mudstone clast conglomerate lags (bypass-dominated facies) (Fig. 10).

Section 2

E2 comprises spill-over fringe deposits (0.4 m thick) overlain by lobe fringe deposits 2 m thick (Figs. 10 and 11). Onlap of basal beds onto underlying mudstones suggests minor (10s of cm to a few meters) seabed topography. E3 includes a basal package of thin-bedded spill-over fringe, abruptly overlain by lenticular, laminated sandstone cut by numerous erosion surfaces that are mantled by cm-scale mudstone clast conglomerates (bypass-dominated facies) (Figs. 10, 12A and 12B). Structured sandstone beds include planar lamination, ripple and climbing ripple lamination, and dewatering structures. Locally, E3 erodes into E2 (Fig. 10).

Figure 13 presents a 20 m long section, which demonstrates detailed bed-scale variations within Section 2. E2 spill-over fringe beds are overlain erosionally by a <0.3 m thick climbing ripple laminated sandstone bed. These are subsequently overlain by thin-bedded siltstones containing multiple erosion surfaces and climbing ripple laminated sandstone beds. The E2 to E3 intra-unit mudstone (0.8 m thick) is removed by irregular erosion surfaces, infilled by structureless medium-grained sandstone, cut by a further erosion surface overlain by thin-bedded siltstones and climbing ripple laminated sandstones. These beds are incised by numerous small (1-20 cm) erosion surfaces that coalesce to form a larger composite surface, draped by thin sandstone beds and mudstone clast conglomerate. A distinctive overlying 1-2 m thick sandstone bed passes from structureless through a division of cm-thick spaced stratification (following Hiscott, 1994) to steepening upward stoss-side preserved climbing ripple lamination. Climbing ripples are progressively sheared and overturned towards the bed top. Basal structureless and stratified sandstone (spaced stratification) (Fig. 12) are interpreted to form under traction carpet conditions (laminar sheared layers; Vrolijk and Southard, 1997) of a rapidly depositing voluminous flow. As flow wanes, sedimentation rates decreases, reducing laminae spacing (Cartigny et al., 2013) and transitioning to climbing ripple laminations (Fig. 10) (Sumner et al., 2008). The increasing angle of climb suggests further waning and increasing suspension fall out rate (Jobe et al., 2012). Sheared and overturned ripples indicate rapid aggradation. These structured sandstone beds, therefore, represent highly aggradational deposits, which are cut by further erosional surfaces, obscuring their depositional morphology and draped by thin lags decreasing in occurrence upwards within laminated siltstone.

Section 3

E2 has an erosional base that removes spill-over fringe deposits (Fig. 10). Localized basal scouring is up to 1 m and draped by a fine-grained sandstone, with large (>15 cm long) rounded mudstone clasts. Overlying the erosion surface, E2 thickens and coarsens upward then thins and fines (Fig. 10). Downdip, beds thin and fine and become mudstone clast-rich, and E2 and E3 amalgamate (Fig. 10). E3 is thinner than in the updip area (Sections 1 and 2), and gradually thins downdip through Section 3 from 2.0 to 0.1 m (Fig. 10). Beds are <15 cm thick, planar laminated, interbedded sandstone and siltstone (Fig. 12C) or slumped and discontinuous with mm-scale mudclasts throughout (Fig. 12D). Numerous erosion surfaces lead to highly irregular tops and bases to beds that thicken and thin abruptly (10s of cm) over meter scale outcrop distances. Discontinuity at the base (Fig. 10) is due to the infilling of erosional topography and truncation. The absence of significant deposition (>2 m) and more evidence of erosion suggests increased sediment bypass compared to Section 2. Overall, there is a fining- and thinning-upward trend, with sandstone beds at the base of E3, and the number of erosion surfaces increasing upwards, suggesting increased sand bypass through the unit (Fig. 10).

Section 4

The D-E mudstone decreases abruptly in thickness from 30 to 11 m over a 60 m outcrop distance (Figs. 10 and 11), and subunits E2 and E3 are offset. The offset does not continue to the top surface of Unit D or the overlying Unit F. Where the D-E mudstone thickness decreases Unit D/E is locally present, thinning out downdip. E2 is locally thicker, with beds thickening and fanning updip and deformed in areas. E3 is also locally thicker and deformed. Both E2 and E3 gradually thin downdip of this area, where the D-E mudstone thickness returns to its updip thickness. This area represents the downdip pinch out of sand-prone E2 lobe deposition, comprising only spill-over fringe downdip (Fig. 11). The thickness and dip changes support the presence of a downdip facing dynamic syn-sedimentary growth fault that decreased D-E mudstone thickness, offset Unit E and soled out within the D-E mudstone. That there is stratigraphic continuity, but thickness changes in all units, suggests that at any one time there was only a minor expression of the fault on the seabed.

Downdip of this area, E3 comprises medium- to thick-bedded lobe deposits with a scoured base and top surface (Figs. 12E, 12F and 12G). The scours on the top surface (1-5 m in length and 0.5-2 m in width), are mantled by cm-scale mudstone clasts and laminated siltstone (Figs. 11 and 12F), interpreted as a lag, and deposits of fine-grained tails of turbidity currents, respectively. The amount of strata removed is unknown, but the bypass assemblage is overlain by fine-grained siltstone that is similar to the background sedimentation (Fig. 12G). Sandstone beds are mudstone clast-rich and moderately deformed, with numerous erosion surfaces throughout (Fig. 12E), suggesting dewatering during deposition and reworking by bypassing flows. Downdip, the sand-prone part of E3 thickens abruptly (9 cm/m) (Fig. 11).

Section 5

E2 comprises spill-over fringe. E3 continues to thicken basinward at a rate of 7 cm/m, attaining a maximum thickness of 40 meters (Figs. 11 and 12H). Updip in Section 5, basal beds of E3 are erosive, overlain by thin mudstone clast lags (Figs. 11 and 12I). Downdip, basal erosion decreases, and a package of tabular climbing ripple laminated sandstone beds is preserved (Fig. 11). These are removed 700 m basinward, and overlain by discontinuous lenticular mud-rich (matrix and clast) sandstone beds (Fig. 11). Overlying this basal package are stratified packages of amalgamated sandstone and sand-rich hybrid beds (Figs. 11, 12H and 12J). Sand-rich hybrid bed packages make up a significant proportion (>50%) of these proximal lobe deposits, but are not present downdip. The abrupt basinward thickening and high sand content is suggestive of rapidly decelerating flows. The erosive features over- and underlying the lobe deposits (Figs. 11 and 12I) are suggestive of deposition in an area of high energy but with temporally fluctuating flow conditions.

Architecture of an exhumed CLTZ

In the Slagtersfontein area, the paleogeographic context between levee and lobe systems (van der Merwe et al., 2014), and the change from updip areas dominated by erosion with widespread evidence for sediment bypass (sections 1-4) to downdip areas dominated by thick sand-prone lobe deposits (Section 5), support the interpretation of a CLTZ in this area during the evolution of E3. Therefore, this area permits a unique opportunity to document a CLTZ and to assess the criteria for their recognition in the rock record. The base of subunit E3 comprises spill-over fringe deposits (Figs. 7, 9 and 10), where not eroded out, which are considered time-equivalent to the sand-rich deposits in the updip intraslope lobe complex (Spychala et al., 2015). This zone is interpreted as sediment bypass-dominated due to minimal amounts of erosion compared to channel systems and limited deposition compared to lobe systems. Subsequently, erosional and depositional elements (*sensu* Mutti and Normark, 1991) in the stratigraphic record are limited in thickness and spatial extent reflecting the dominance of sediment bypass. The assemblage of erosional and depositional elements in Sections 2-4 in subunit E3 are synthesized here.

Erosional elements

Isolated and composite erosional features are numerous in the form of relatively flat surfaces and concave scours. Scours throughout the Slagtersfontein CLTZ are generally composite >2 m deep features. Larger scale features cut though the E2-E3 intra-unit mudstone and into Unit E2 and are rarely >3 m deep (Figs. 10 and 11). The irregular shaped scours are draped by a combination of lag deposits and thin-bedded siltstone. The amalgamation and 2D view of these features means their morphology cannot be constrained accurately. Scours on top of sandstone beds are 1-5 m in length and up to several m in width (van der Merwe et al., 2014), often display asymmetry with steeper headwalls, and are interpreted as megaflutes (e.g. Elliott, 2000). They form individual and composite features on large-scale deflation surfaces (Fig. 11), interpreted to represent prolonged periods of weakly confined sediment bypass, which extend many kilometers (Fig. 7C). The lack of significant incision (>3 m deep) suggests widespread scouring rather than channel development, although the presence of shallow high aspect ratio channels is possible, where flows locally became more confined. The lack of deeper scour features (e.g. Hofstra et al., 2015) suggests flows were not sufficiently concentrated in a single location and temporally fluctuated between deposition, bypass and erosion. The Slagtersfontein CLTZ, although evidently in a fairly axial environment (indicated by the high energy nature of deposits, erosion and scours), is likely lateral to the main position of channel propagation given the presence of external levees and absence of main channel-fills, therefore mega-scours (e.g. Hofstra et al., 2015) may be present out of section.

Depositional elements

Mudstone clast conglomerates, interpreted as lag deposits, are common throughout the Slagtersfontein CLTZ (Figs. 10, 11 and 13). The clasts are likely sourced from the widespread E2-E3 mudstone, with a large range of clast sizes and roundness suggesting different transport distances and/or rheology. Poorly sorted lenses of mudstone and medium-grained sandstones are also interpreted as 'coarse-grained' lag deposits as this grain-size is otherwise exceptionally rare in the Fort Brown Fm. Aggradational beds are recognized in the proximal areas of the CLTZ, with spaced, climbing ripple and sheared climbing ripple lamination. These aggradational beds are present stratigraphically and spatially between coalesced scours and bypass lags (Fig. 12), for outcrop lengths up to 20 m, with their original depositional morphology and extent unknown. These beds therefore may represent rapidly depositing sheets from unconfined flows, and/or long wavelength aggradational bedforms with the latter similar to sediment waves (e.g. Wynn and Stow, 2002; Wynn et al., 2002a, 2002b; Cartigny et al., 2011; Symons et al., 2016). Small-scale slumping and dewatering structures, especially in thick amalgamated sandstone beds, are common throughout the CLTZ (sections 2-5, Figs. 10 and 11), suggesting rapid deposition due to flow deceleration followed by liquefaction whilst flows continued.

Hybrid beds are not generally associated with proximal lobe settings (Haughton et al., 2003, 2009; Hodgson, 2009), but are common immediately downdip of the CLTZ in the proximal lobe (Section 5). Sand-rich hybrid bed occurrence solely in this location may be a direct result of the CLTZ. As sand-rich, high energy, flows traverse the scoured, mud-rich zone, the downdip transformation from non-cohesive to more cohesive flow may be driven by incorporation of mud and mudstone clasts via erosion, damping turbulence (Baas and Best, 2002; Amy and Talling, 2006), and producing high-concentration to pseudo-laminar flow conditions (Talling et al., 2004; Ito, 2008; Baas et al., 2011). The sharp contact between the upper and lower division of the hybrid beds suggests the flow had partitioned into cohesive and non-cohesive components. Mudstone clasts present in the tops of the lower division, are aligned with flow, suggesting transport by turbulent mechanisms, with clasts likely supported in the rear of the flow (Hodgson, 2009). The lack of mud suggests finer portions of turbidity currents and less-cohesive, mud-rich debris flows, may have bypassed this axial area and continued onwards to form the silt-rich hybrid beds recognized in lateral lobe fringes. Although not typically associated with proximal lobes, hybrid bed rich strata have been noted as occurring in highly aggradational phases of fan development, and phases of channel propagation (Haughton et al., 2009).

DISCUSSION

Evolution of slope profile

Evidence for intraslope lobe complexes (Spychala et al., 2015) and widespread spill-over fringe deposits, shows that E2 and E3 deposition in the study area commenced when flows had healed updip slope accommodation and were able to bypass downdip. The Slagtersfontein CLTZ is therefore interpreted as forming in a base of slope area between a higher gradient 'ramp' (*sensu* Prather, 2003; Prather et al., 2017) and a lower gradient 'step' (*sensu* O'Byrne et al., 2004) (Fig. 14). No evidence of further topographic influence to the east, with lobe deposits gradually thinning and pinching out over a further 40 kms (van der Merwe et al., 2014) indicates that this was the basin-floor. The presence of syn-sedimentary faulting supports deposition above an unstable ramp in a base of slope area. Growth faulting due to sediment instability is common in submarine slope settings (Galloway, 1986), and possibly nucleated in this location as a result of differential compaction over the margin of a Unit D sandstone-filled channel complex immediately below. The rate of change in facies and thickness in Slagtersfontein, and presence of the fault, suggests that the change from slope to basin-floor was sharp, and may have formed an abrupt break-in-slope.

Key areas of basinward thickening and abrupt change in facies in Unit D/E, and subunits E2 and E3 is identified in multiple correlation panels in similar locations (Fig. 9), suggesting a long lived break-in-slope position. The 10 km distance between panels 2 and 1 marks a key change in facies and architecture across-strike in subunit E3. The facies and thickness changes in the north are gradual with some interfingering of levee and lobe deposits, followed by a gentle thickening of lobes, marking a levee-lobe transition zone. This compares with steeper and/or more incised morphology in the Slagtersfontein area, suggesting a highly variable base of slope physiography across strike (Fig. 14).

Spatial variability and evolution of the CLTZ

Across-strike and downdip variations have been noted throughout the E3 CLTZ. The maximum strike width of the CLTZ measured as the distance between panels 1 and 3, is 11 kilometers (restored). This extends to a maximum of around 14 km in width where the CLTZ scour surfaces extend laterally and are present across the top surface of E3 to the South (panels 3 and 4, Figs. 7C, 7D, 8 and 9C).

More variation in the character and extent of the CLTZ has been recorded in dip section, illustrated in four time slices (Fig. 15). At T1 the CLTZ was approximately 3 km in dip length with a minimum 2 m thick lobe deposit downdip (Fig. 11). Subsequently (T2), the CLTZ lengthened to approximately 4 km, with T1 deposits partially eroded and the area of deposition moving basinward (Fig. 11). During T3, the CLTZ shortened to approximately 2 km, with lobe deposition above the composite T2 erosion surface (Fig. 11). A final lengthening of the CLTZ (T4) to approximately 3.5 km along this 2D section, but expanding to at least 6 km across strike to the south, resulted in the formation of the youngest scoured surface that accentuates the rate of basinward thickening of the proximal lobe deposits (Fig. 11), and creates the most widespread scour surface (Fig. 7). The absence of levee deposits under- or overlain by bypass indicators (Fig. 10), suggests this is the most updip expression of the CLTZ. The CLTZ migration evident at Slagtersfontein reflects the minimum amount of migration in the zone, with evidence of additional fluctuations likely lost due to later erosion, and observations restricted by outcrop constraints across strike.

Influence of physiography and flow dynamics through time

This study documents depositional strike variability in the downdip transition from channel-levee systems to lobe complexes. The dominant controls on the lateral variation within the system are considered to be physiographic changes along the base of slope and variations in flow dynamics through time. The formation of features such as scour fields have been associated with the occurrence of hydraulic jumps, commonly occurring within base of slope areas where changes in gradient and flow confinement lead to flows changing from supercritical to subcritical (Mutti and Normark, 1987, 1991; Weirich, 1989; Kostic and Parker, 2006; Sumner et al., 2013). Downdip reacceleration of flows suggests that flows can repeatedly become supercritical across the CLTZ, resulting in multiple hydraulic jumps (Sumner et al., 2013; Dorrell et al., 2016). Incoming flows are more likely to be supercritical where they have traversed areas of steeper gradient. This suggests that a higher gradient slope was present updip of Slagtersfontein, which may have resulted in incoming flows being supercritical, and more likely to undergo hydraulic jump when they reached the base of slope.

Experimental studies have shown that increasing the slope angle updip of a break in slope can lengthen the geographical zone in which hydraulic jumps occur (Kostic and Parker, 2006). A larger magnitude break-in-slope will result in greater changes in the level of turbulence at the initial hydraulic jump, creating a greater reduction in flow velocity and increasing scouring (Lee et al., 2002). The slope gradient will vary temporally, for example shallowing through erosion, thus changing these conditions. Flows are more likely to be supercritical in axial locations (e.g. Slagtersfontein) in close proximity to the feeder channel, where they are subject to higher concentrations and velocities. Therefore, the criticality of the incoming flow at a single location will vary temporally with migrations or avulsions in the feeder system. Changes in flow magnitude may also be expected to affect the dip extent of the CLTZ (Fig. 15). Flows with larger amounts of suspended sediment will be able to reach greater velocities, shifting the position of the hydraulic jump zone farther downdip (Kostic and Parker, 2006). Larger amounts of suspended sediment will also increase flow stratification, which has been shown to cause flows to undergo hydraulic jumps at depth averaged Froude numbers lower than 1 (Waltham, 2004; Huang et al., 2009; Sumner et al., 2013; Dorrell et al., 2016). Variations in flow and sediment input may therefore control the locations and spread of hydraulic fluctuations and ultimately the CLTZ location and dimensions.

Temporal evolution within the system (e.g. modifications of slope gradient, flow/deposit interactions) will also influence the size and location of the CLTZ, affecting the flow pathways and sediment routing, leading to different stages of development such as those noted in this study. If system input is stable, channel-levee systems will eventually adjust to the equilibrium profile (Pirmez et al., 2000; Kneller, 2003; Covault et al., 2016). As the system matures and becomes more efficient, a higher proportion of flows with a larger amount of their initial sediment load will reach the base of slope (Hodgson et al., 2016). This may result in a basinward migration of the CLTZ or increase in CLTZ length with deposition tending to occur further downdip of the feeder channel-mouth in efficient systems compared to more inefficient systems (Mutti and Normark, 1987). Conversely, periods of channel aggradation (e.g. Hodgson et al., 2011; Covault et al., 2016), may decrease downdip sediment supply thereby reducing the size of the CLTZ. Therefore, the spatial extent of the CLTZ may relate to phases of higher and lower efficiency in the channel system.

Accommodation changes across the slope will also affect the size of flows and the amount of material reaching the base of slope (e.g. Meckel et al., 2002; Smith, 2004b; Hay, 2012; Marini et al., 2015). Updip intraslope lobe accommodation (Spychala et al., 2015) restricted the supply of sediment downdip. The initial coarse-grained deposits (T1) represent the first flows that were able to bypass their coarser component over healed accommodation, down the ramp, and onto the basin-floor. As intraslope accommodation was healed, higher energy flows bypassed downdip to form thicker and coarser deposits (T3).

Individual flow scale variability within the CLTZ

As well as the large-scale changes in the spatial extent of the CLTZ, variability at the scale of individual flows may contribute to the distribution of features. Overall, the exhumed CLTZ records the interplay of erosional and depositional processes and bedform / sheet-deposit development laterally over meter-scale distances. There are no discrete areas within the stratigraphic expression of the CLTZ of dominantly large-scale erosion (e.g. composite scouring) or deposition (e.g. sediment waves), as suggested in previous models (e.g. Wynn et al., 2002a). Studies of the modern seabed have shown that processes are dynamic, with adjacent scours simultaneously eroding and being filled due to density currents undergoing hydraulic jumps at different spatial locations (Macdonald et al., 2011a; Sumner et al., 2013). As noted previously, submarine density currents can form a region of scattered hydraulic jumps as they undergo the transition from supercritical to subcritical at different points (Sumner et al., 2013; Dorrell et al., 2016) through spatially variable flow-relief interactions (e.g. Groenenberg et al., 2010) and/or through waxing and waning of individual flows (Dorrell et al., 2016). This region of scattered hydraulic jumps would create strong vertical uplift, keeping sediment in suspension (over the CLTZ), delaying abrupt sediment deposition, and creating a field of scours (Wynn et al., 2002a; Dorrell et al., 2016). For flows with low Froude numbers the flow dynamics of successive hydraulic jumps have been shown to maintain basal shear stress and sediment transport across a CLTZ. This enables large-scale deposition to occur immediately downstream of the CLTZ, forming sediment waves and thick, dewatered proximal lobe deposits (Dorrell et al., 2016). However, localized erosion and deposition at individual jumps will lead to small-scale topographic variations on the seabed with subsequent turbidity currents encountering a more marked change or reversal in slope aspect (Lee et al., 2002). This will result in spatial variations of bed shear stress related to flow-topography interactions (e.g. Agadir basin, Macdonald et al., 2011a). Therefore, over short timescales without the need of CLTZ migration, both erosional and depositional processes are likely to occur within the same zone (Fig. 16A), due to fluctuations in flow conditions and interaction with a dynamic seabed topography.

Comparison to other CLTZs

Key variables in determining formation of a CLTZ (e.g. the magnitude of slope break and the mud content within the flows) have been considered by other studies (Mutti and Normark, 1987; Wynn et al., 2002a). As demonstrated in this study, these factors can vary spatially from axial to margin flow positions and temporally due to changes in flow dynamics and topographical controls within a single system. Systems on continental margins show CLTZ lengths of 30-120 kilometers (Kenyon and Millington, 1995; Kenyon et al., 1995; Palanques et al., 1995; Morris et al., 1998; Wynn et al., 2002a). Wynn et al. (2002a) documented a relationship between the length of the CLTZ and the size and type of the turbidite system. Table 2 (modified from Wynn et al. (2002a) to include this study) indicates that the E3 CLTZ has a length and basin/fan area comparable to the Navy Fan (Normark et al., 1979; Wynn et al., 2002a) but an order of magnitude smaller to all others (Kenyon and Millington, 1995; Kenyon et al., 1995; Palanques et al., 1995; Morris et al., 1998; Wynn et al., 2002a). A key similarity between E3 and the Navy Fan is their sand-rich nature with all other CLTZs interpreted to have formed in comparatively more silt-rich systems (Wynn et al., 2002a). Flows in mud-rich systems will be more efficient (Mutti, 1992; Gladstone et al., 1998), promoting sediment bypass and the formation of more longitudinally extensive CLTZs (Mutti and Normark, 1987). The greater flow thickness and enhanced stratification of mud-rich flows may also lead to hydraulic jumps only occurring in the lower part of the flow, with the upper flow bypassing the jumps, again enhancing the degree of sediment bypass (Dorrell et al., 2016) and aiding the development of more extensive CLTZs. As well as the sand to mud ratio, the scale of the feeder system is considered to influence the size of CLTZs (Mutti and Normark, 1987), with larger feeder channels associated with larger amounts of suspended sediment and greater flow velocities extending the zone of hydraulic jumps (Kostic and Parker, 2006) to form larger CLTZs (Mutti and Normark, 1987; Wynn et al., 2002a). Another key variable is the gradient change at the base of slope. The magnitude, incoming gradient and length of the slope break will influence flow conditions, and therefore the size of the CLTZ. Although an absolute slope angle cannot be measured from this study, slope breaks from other systems with CLTZ indicate only a small magnitude (<1º) change is needed (e.g. Kenyon et al., 1995, 0.6º - 0.3º).

A generic model for CLTZ stratigraphic architecture

This outcrop study expands upon the findings of previous studies of exhumed CLTZs (Mutti and Normark, 1987; Wynn et al., 2002a; Pemberton et al., 2016). Most significantly, that CLTZs are not fixed and can expand or contract, and migrate several kilometers. Datasets from modern and active systems are unable to capture this variability through time, and previous outcrop datasets have been limited in palaeogeographic constraint. Moreover, this study demonstrates a juxtaposition of depositional and erosional elements within the CLTZ, rather than separation into discrete zones. This may partially be a factor of the migration of the zone due to allogenic and autogenic controls described above as well as preservation potential, but recent observations of the modern seabed (Macdonald et al., 2011a; Dorrell et al., 2016) and monitoring of active systems (e.g. Hughes Clark et al., 2012) suggest zones of mixed erosional and depositional bedforms may be forming instantaneously.

The areas of most intense reworking (numerous erosional surfaces, scours and bypass lags) across Slagtersfontein are in the updip area of the CLTZ, in closest proximity to the mouth of the feeder channel (Figs. 10 and 11). Figure 16 demonstrates how stratigraphic surfaces form within a CLTZ, and how minimal deposition and composite erosion surfaces can represent several stages of migration, expansion and contraction of a CLTZ. Distally and laterally away from the axial areas, deposits show less reworking and preserve comparatively more individual geomorphic features. The unique preservation of the Slagtersfontein CLTZ, unaffected by later stage progradation and incision of the channel system, suggests this section is either: (i) a sufficiently off-axis transect through the CLTZ and was not cannibalized as the channel propagated (Hodgson et al., 2016); or (ii) underdeveloped and the channel never fully propagated through the zone (Hofstra et al., 2015). Given the evidence for high-energy erosion and deposition, the spatial control on system position, and the absence of overlying external levee deposits, the partially developed model is favored. An abrupt system shutdown may have been caused by channel avulsion or an abrupt decrease in regional sediment supply, as the upper surface is draped by a system-wide hemipelagic mudstone.

The stratigraphic expression of CLTZs has been poorly constrained to date, with models consisting of composite surfaces separating underlying lobes from overlying channels (Gardner et al., 2003; Pyles et al., 2014), the identification of individual features (Mutti and Normark, 1987), or lenticular bodies infilling scours (Pemberton et al., 2016). This study demonstrates how CLTZs can migrate and change their planform geometry in response to spatially and temporally variable flow dynamics and topographic controls. This results in highly variable and composite stratigraphic surfaces and the juxtaposition of distinctive erosional and depositional elements to form complicated stratigraphic successions. The dynamic nature of a CLTZ documented here, within a tightly constrained regional stratigraphic framework, enables a generic model of CLTZ transfer into the stratigraphic record to be constructed for the first time (Fig. 16).

Key characteristics of the model are outlined in Table 3. Many of these features have been documented previously in outcrop and modern seabed datasets, indicating that the model can be widely applied, although the specific characteristics will be expressed differently. For example, the Fort Brown Formation has a limited grain-size range (silt to upper fine sand), with lag deposits identified by the presence of lower medium sand. In systems with a wider grain-size, lag deposits would be represented by a wider grain-size range, and be less well sorted. The depths of scours in this study are significantly smaller than others documented in modern CLTZs, this may reflect an off-axis exposure of the CLTZ, or be related to the size of the feeder system. In modern seabed datasets, coarse grained sediment waves orientated perpendicular to flow direction have been identified (e.g. Morris et al. 1998; Wynn et al., 2002b), but these depositional bedforms remain elusive in outcrop record.

This range of features forms a characteristic assemblage, enabling recognition of CLTZ zones at outcrop and possibly sub-surface. It is important to recognize that end-member models are possible, for instance that presented by Pemberton et al. (2016) where sandstones infill a zone of complex scours producing lenticular sand bodies. In comparison, the model presented herein represents a dynamic CLTZ producing a far more spatially variable and heterogeneous sedimentary infill. This model may represent the norm for many CLTZs with lack of spatial variability recognized in other studies likely a factor of outcrop constraints.

CONCLUSIONS

This study reports the first detailed stratigraphic expression of a long-lived and well-preserved bypass-dominated CLTZ at outcrop. Exceptional paleogeographic context of the system uniquely allows dip and lateral constraints on dimensions through time. With previous studies primarily focused on modern seabed data, the temporal variability in CLTZ evolution documented here allows development of the first dynamic CLTZ model. This model encompasses: lateral variability; sedimentological recognition criteria; expansion, contraction and migrations of the zone; and transfer into the stratigraphic record. Lateral variations across the base of slope include transition from, inter-fingering levee to lobe deposits off-axis in the system, to a bypass-dominated CLTZ in a more proximal area. This variation is considered to be the result of physiographic changes and variations in flow dynamics across the base of slope. Key recognition criteria for CLTZs have been established including: scours, composite erosional surfaces, bypass lags, and remnant rapidly unconfined sheets/ sediment waves. In addition, previously undocumented, abundant sand-rich hybrid beds are recognized in proximal lobe deposits downdip of the CLTZ. Overall the CLTZ is a dynamic area, with interactions of different parameters including physiography (both in slope gradient and shape), flow magnitude and character, and the position and extent of channel confinement. This results in changes in the dip and strike extent (maximum 14 km in strike and 6 km in dip), and geometry of the CLTZ and creates a distinct area of juxtaposed remnant erosional and depositional features. The consequence of this dynamic character is a complicated and composite transfer of the CLTZ into the stratigraphic record.

ACKNOWLEDGEMENTS

The authors thank the local farmers of the Laingsburg region for permission to undertake field studies on their land, especially Henk Steyn. We thank Catherine Burns, Geoff Reith, Sarah Cobain, Lewis Burden, Sophie Cullis and Grace Cosgrove for field assistance. Christopher Stevenson is thanked for discussions. This work was carried out as part of the

SLOPE 4 consortium research project. We are grateful for financial support from: Anadarko, BHP Billiton, BP, ConocoPhillips, ENGIE, Maersk Oil, Murphy, Nexen, Petrobras, Premier Oil, Shell, Statoil, Total, VNG Norge and Woodside. The authors would also like to thank two anonymous reviewers, Andrea Fildani, Steve Hubbard and editor David Schofield for their insightful comments and helpful suggestions which have significantly improved the manuscript.

REFERENCES

Adeogba, A.A., McHargue, T.R., and Graham, S.A., 2005, Transient fan architecture and depositional controls from near-surface 3-D seismic data, Niger Delta continental slope: AAPG Bulletin, v. 89, p. 627–643.

Allen, J.R.L., 1970, A quantitative model of climbing ripples and their cross-laminated deposits: Sedimentology, v. 14, p. 5-26, doi: 10.1111/j.1365-3091.1970.tb00179.

Allen, J.R.L., 1984, Parallel lamination developed from upper-stage plane beds: a model based on the larger coherent structures of the turbulent boundary layer: Sedimentary Geology, v. 39, p. 227-242, doi: 10.1016/0037-0738(84)90052-6.

Allen, J.R.L., 1985, Principles of Physical Sedimentology: London, Allen and Unwin, p.196.

Allen, J.R.L., and Banks, N.L., 1972, An interpretation and analysis of recumbent folded deformed cross-bedding: Sedimentology, v. 19, p. 257-283.

Amy, L.A., and Talling, P.J., 2006, Anatomy of turbidites and linked debrites based on long distance (120× 30 km) bed correlation, Marnoso Arenacea Formation, Northern Apennines, Italy: Sedimentology, v. 53, p. 161-212, doi: 10.1111/j.1365-3091.2005.00756.x.

Baas, J.H., and Best, J.L., 2002, Turbulence modulation in clay-rich sediment-laden flows and some implications for sediment deposition: Journal of Sedimentary Research, v. 72, p. 336-340, doi: 10.1306/120601720336.

Baas, J.H., Best, J.L., and Peakall, J., 2011, Depositional processes, bedform development and hybrid bed formation in rapidly decelerated cohesive (mud–sand) sediment flows: Sedimentology, v. 58, p. 1953-1987, doi: 10.1111/j.1365-3091.2011.01247.x.

Beaubouef, R.T., 2004, Deep-water leveed-channel complexes of the Cerro Toro Formation, Upper Cretaceous, southern Chile: American Association of Petroleum Geologists, Bulletin, v. 88, p. 1471-1500, doi: 10.1306/06210403130.

Beaubouef, R.T., Rossen, C., Zelt, L.B., Sullivan, M.D., Mohrig, D.C., and Jennette, D.C., 1999, Deep-water sandstones, Brushy Canyon Formation, West Texas: AAPG Continuing Education Course Note Series no. 40, The American Association of Petroleum Geologists, p. 48.

Bouma, A., 1962, Sedimentology of some flysch deposits. A graphic approach to facies interpretation: Amsterdam, Elsevier, p. 168.

Brunt, R.L., Di Celma, C.N., Hodgson, D.M., Flint, S.S., Kavanagh, J.P., and van der Merwe, W.C., 2013a, Driving a channel through a levee when the levee is high: An outcrop example of submarine downdip entrenchment: Marine and Petroleum Geology, v. 41, p. 134-145, doi: 10.1016/j.marpetgeo.2012.02.016.

Brunt, R.L., Hodgson, D.M., Flint, S.S., Pringle, J.K., Di Celma, C., Prélat, A., and Grecula, M., 2013b, Confined to unconfined: Anatomy of a base of slope succession, Karoo Basin, South Africa: Marine and Petroleum Geology, v. 41, p. 206-221, doi: 0.1016/j.marpetgeo.2012.02.007.

Cartigny, M.J.B., Postma, G., Van Den Berg, J.H., and Mastbergen, D.R., 2011, A comparative study of sediment waves and cyclic steps based on geometries, internal structures and numerical modeling: Marine Geology, v. 280, p. 40-56, doi: 10.1016/j.margeo.2010.11.006.

Cartigny, M.J.B., Eggenhuisen, J.T., Hansen, E.W.M., and Postma, G., 2013, Concentration-dependent flow stratification in experimental high-density turbidity currents and their relevance to turbidite facies model: Journal of Sedimentary Research, v. 83, p. 1046-1064, doi: 10.1130/G35957.1.

Catuneanu, O., Hancox, P.J., and Rubidge, B.S., 1998, Reciprocal flexural behaviour and contrasting stratigraphies: a new basin development model for the Karoo retroarc foreland system, South Africa: Basin Research, v. 10, p. 417–439, doi: 10.1046/j.1365-2117.1998.00078.x.

Chapin, M.A., Davis, V.P., Gibson, J.L., and Pettinghill, H.S., 1994, Reservoir architecture of turbidite sheet sandstones in laterally extensive outcrops, Ross Formation, western Ireland, *in* Weimer, P., Bouma, A.H., and Perkins, B.F., eds., Submarine Fans and Turbidite Systems: Gulf Coast Section SEPM 15^{th} Annual Research Conference, 15th, p. 53–68.

Cobain, S., Peakall, J., and Hodgson, D.M., 2015, Indicators of propagation direction and relative depth in clastic injectites: Implications for laminar versus turbulent flow processes: Geological Society of America Bulletin, v. 127, p. 1816-1830, doi: 10.1130/B31209.1.

Covault, J.A., Sylvester, Z., Hubbard, S.M., Jobe, Z.R., and Sech, R.P., 2016, The stratigraphic record of submarine-channel evolution: The Sedimentary Record, v. 14, p. 4-11.

Covault, J.A., Kostic, S., Paull, C.K., Sylvester, Z., and Fildani, A., 2017, Cyclic steps and related supercritical bedforms: Building blocks of deep-water depositional systems, western North America: Marine Geology, v. 393, p. 4-20, doi: 10.1016/j.margeo.2016.12.009

Deptuck, M.E., Sylvester, Z., Pirmez, C., and O'Byrne, C., 2007, Migration-aggradation history and 3-D seismic geomorphology of submarine channels in the Pleistocene Benin-major Canyon, western Niger Delta slope: Marine and Petroleum Geology, v. 24, p. 406-433.

Di Celma, C., Brunt, R.L., Hodgson, D.M., Flint, S.S., and Kavanagh, J.P., 2011, Spatial and temporal evolution of a Permian submarine slope channel-levee system, Karoo Basin, South Africa: Journal of Sedimentary Research, v. 81, p. 579-599, doi: 10.2110/jsr.2011.49.

Dorrell, R.M., Peakall, J., Sumner, E.J., Parsons, D.R., Darby, S.E., Wynn, R.B., Özsoy, E., and Tezcan, D., 2016, Flow dynamics and mixing processes in hydraulic jump arrays: Implications for channel-lobe transition zones: Marine Geology, v. 381, p. 181-193.

Elliott, T., 2000, Megaflute erosion surfaces and the initiation of turbidite channels: Geology, v. 28, p. 119–122.

Figueiredo, J., Hodgson, D.M., and Flint, S.S., 2010, Depositional environments and sequence stratigraphy of an exhumed Permian mud-dominated submarine slope succession, Karoo basin, South Africa: Journal of Sedimentary Research, v. 80, p. 97-118, doi: 10.2110/jsr.2010.002.

Figueiredo, J.P., Hodgson, D.M., Flint, S.S., and Kavanagh, J.P., 2013, Architecture of a channel complex formed and filled during long-term degradation and entrenchment on the upper submarine slope, Unit F, Fort Brown Fm., SW Karoo Basin, South Africa: Marine and Petroleum Geology, v. 41, p. 104-116, doi: 10.1016/j.marpetgeo.2012.02.006.

Fildani, A., and Normark, W.R., 2004, Late Quaternary evolution of channel and lobe complexes of Montery Fan: Marine Geology, v. 206, p. 199-223, doi: 10.1016/j.margeo.2004.03.001.

Flint, S.S., Hodgson, D.M., Sprague, A.R., Brunt, R.L., van der Merwe, W.C., Figueiredo, J., Prélat, A., Box, D., Di Celma, C., and Kavanagh, J.P., 2011, Depositional architecture and sequence stratigraphy of the Karoo basin floor to shelf edge succession, Laingsburg depocentre, South Africa: Marine and Petroleum Geology, v. 28, p. 658–674, doi: 10.1016/j.marpetgeo.2010.06.008.

Galloway, W.E., 1986, Growth faults and fault-related structures of prograding terrigenous clastic continental margins: Gulf Coast Association of Geological Societies Transactions, v. 36, p. 121-128.

Gamberi, F., and Rovere, M., 2011, Architecture of a modern transient slope fan (Villafranca fan, Gioia basin—Southeastern Tyrrhenian Sea): Sedimentary Geology, v. 236, p. 211–225.

Gardner, M.H., Borer, J.A., Melick, J.J., Mavilla, N., Dechesne, M., and Wagerle, R.N., 2003, Stratigraphic process–response model for submarine channels and related features from studies of Permian Brushy Canyon outcrops, West Texas: Marine and Petroleum Geology, v. 20, p. 757–787, doi: 10.1016/j.marpetgeo.2003.07.004.

Gladstone, C., Phillips, J.C., and Sparks, R.S.J., 1998, Experiments on bidisperse, constant-volume gravity currents; propagation and sediment deposition: Sedimentology, v. 45, p. 833-843.

Groenenberg, R.M., Hodgson, D.M., Prélat, A., Luthi, S.M., and Flint, S.S., 2010, Flow–deposit interaction in submarine lobes: insights from outcrop observations and realizations of a process-based numerical model: Journal of Sedimentary Research, v. 80, p. 252-267, doi: 10.2110/jsr.2010.028.

Haughton, P.D., Barker, S.P., and McCaffrey, W.D., 2003, ‘Linked’ debrites in sand-rich turbidite systems–origin and significance: Sedimentology, v. 50, p. 459-482, doi: 10.1046/j.1365-3091.2003.00560.x.

Haughton, P., Davis, C., McCaffrey, W., and Barker, S., 2009, Hybrid sediment gravity flow deposits classification, origin and significance: Marine and Petroleum Geology, v. 26, p. 1900-1918, doi: 10.1046/j.1365-3091.2003.00560.x.

Hay, D., 2012, Stratigraphic evolution of a tortuous corridor from the stepped slope of Angola, *in* Prather, B.E., Deptuck, M.E., Mohrig, D.C., van Hoorn, B., and Wynn, R.B., eds., Application of the Principles of Seismic Geomorphology to Continental-Slope and Base-of-Slope Systems: Case Studies from Seafloor and Near-Seafloor Analogues, SEPM Special Publication, v. 99, p. 163-180, doi: 10.2110/pec.12.99.0163.

Hiscott, R.N., 1994, Traction-carpet stratification in turbidites- Fact or Fiction?: Journal of Sedimentary Research, v. A64, p. 204-208, doi: 10.1306/D4267D57-2B26-11D7-8648000102C1865D.

Hiscott, R.N., and Middleton, G.V., 1980, Fabric of coarse deep-water sandstones, Tourelle Formation, Quebec, Canada: Journal of Sedimentary Petrology, v. 50, p. 703-722.

Hiscott, R.N., Hall, F.R., and Pirmez, C., 1997, Turbidity-current overspill from the Amazon channel: texture of the silt/sand load, paleoflow from anisotropy of magnetic susceptibility and implications for flow processes, *in* Flood, R.D., Piper, D.J.W., Klaus, A., and Peterson, L.C., eds., Proceedings of the Ocean Drilling Program, Scientific Results 155, Ocean Drilling Program, College Station, Texas, p. 53–78.

Hodgson, D.M., 2009, Origin and distribution of bipartite beds in sand-rich submarine fans: Constraints from the Tanqua depocentre, Karoo Basin, South Africa: Marine and Petroleum Geology, v. 26, p. 1940–1956, doi: 10.1016 /j.marpetgeo.2009.02.011.

Hodgson, D.M., Di Celma, C., Brunt, R.L., and Flint, S.S., 2011, Submarine slope degradation and aggradation and the stratigraphic evolution of channel-Levee systems: Journal of the Geological Society, v. 168, p. 625-628, doi: 10.1144/0016-76492010-177.

Hodgson, D.M., Kane, I.A., Flint, S.S., Brunt, R.L., and Ortiz-Karpf, A., 2016, Time-transgressive confinement on the slope and the progradation of basin-floor fans: Implications for the sequence stratigraphy of deep-water deposits: Journal of Sedimentary Research, v. 86, p. 73-86, doi: 10.2110/jsr.2016.3.

Hofstra, M., Hodgson, D.M., Peakall, J., and Flint, S.S., 2015, Giant scour-fills in ancient channel-lobe transition zones: Formative processes and depositional architecture: Sedimentary Geology, v. 329, p. 98-114, doi: 10.1016/j.sedgeo.2015.09.004.

Huang, H., Imran, J., Pirmez, C., Zhang, Q. and Chen, G., 2009, The critical densimetric Froude number of subaqueous gravity currents can be non-unity or non-existent: Journal of Sedimentary Research, v. 79, p.479-485.

Hughes Clarke, J.E., Brucker, S., Muggah, J., Hamilton, T., Cartwright, D., Church, I, and Kuus, P., 2012, Temporal progression and spatial extent of mass wasting events on the Squamish prodelta slope, *in* Eberhardt, E., Froese, C., Turner, A.K., and Leroueil, S. eds., Landslides and Engineered Slopes: Protecting Society through Improved Understanding, p. 1091-1096.

Ito, M., 2008, Downfan transformation from turbidity currents to debris flows at a channel-to-lobe transitional zone: the lower Pleistocene Otadai Formation: Journal of Sedimentary Research, v. 78, p. 668–682, doi: 10.2110/jsr.2008.076.

Jobe, Z.R., Lowe, D.R., and Morris, W.R., 2012, Climbing-ripple successions in turbidite systems: depositional environments, sedimentation rates and accumulation times: Sedimentology, v. 59, p. 867- 898, doi: 10.1111/j.1365-3091.2011.01283.x.

Johnson, S.D., Flint, S., Hinds, D., and De Ville Wickens, H., 2001, Anatomy, geometry and sequence stratigraphy of basin floor to slope turbidite systems, Tanqua Karoo, South Africa: Sedimentology, v. 48, p. 987-1023, doi : 10.1046/j.1365-3091.2001.00405.x.

Jones, G.E.D., Hodgson, D.M., and Flint, S.S., 2015, Lateral variability in clinoform trajectory, process regime, and sediment dispersal patterns beyond the shelf-edge rollover in exhumed basin margin-scale clinothems: Basin Research, v. 27, p. 657-680, doi: 10.1111/bre.12092.

Kane, I.A., and Hodgson, D.M., 2011, Sedimentological criteria to differentiate submarine channel levee subenvironments: Exhumed examples from the Rosario Fm. (Upper Cretaceous) of Baja California, Mexico, and the Fort Brown Fm. (Permian), Karoo Basin, S. Africa: Marine and Petroleum Geology, v.28, p.807-823. doi: 10.1016/j.marpetgeo.2010.05.009

Kane, I.A., Kneller, B.C., Dykstra, M., Kassem, A., and McCaffrey, W.D., 2007, Anatomy of a submarine channel-levee: an example from Upper Cretaceous slope sediments, Rosario Formation, Baja California, Mexico: Marine and Petroleum Geology, v. 24, p. 540-563. doi:10.1016/j.marpetgeo.2007.01.003.

Kenyon, N.H., and Millington, J., 1995, Contrasting deep-sea depositional systems in the Bering Sea, *in* Pickering, K.T., Hiscott, R.N., Kenyon, N.H., Ricci Lucchi, F., and Smith, R.D.A., eds., Atlas of Deep Water Environments: Architectural Style in Turbidite Systems: London, Chapman and Hall, p. 196-202.

Kenyon, N.H., Millington, J., Droz, L., and Ivanov, M.K., 1995, Scour holes in a channel-lobe transition zone on the Rhone cone, *in* Pickering, K.T., Hiscott, R.N., Kenyon, N.H., Ricci Lucchi, F., and Smith, R.D.A., eds., Atlas of Deep Water Environments: Architectural Style in Turbidite Systems: London, Chapman and Hall, p. 212-215.

Kneller, B., 2003, The influence of flow parameters on turbidite slope channel architecture: Marine and Petroleum Geology, v. 20, p. 901–910, doi: 10.1016/j.marpetgeo.2003.03.001.

Kneller, B.C., and Branney, M.J., 1995, Sustained high-density turbidity currents and the deposition of thick massive sands: Sedimentology, v. 42, p. 607-616, doi: 10.1111/j.1365-3091.1995.tb00395.x.

Kostic, S., and Parker, G., 2006, The response of turbidity currents to a canyon–fan transition: internal hydraulic jumps and depositional signatures: Journal of Hydraulic Research, v. 44, p. 631-653, doi: 10.1080/00221686.2006.9521713.

Lee, S.E., Talling, P.J., Ernst, G.G., and Hogg, A.J., 2002, Occurrence and origin of submarine plunge pools at the base of the US continental slope: Marine Geology, v. 185, p. 363-377, doi: 10.1016/S0025-3227(01)00298-5.

Lowe, D.R., 1982, Sediment gravity flows: II Depositional models with special reference to the deposits of high-density turbidity currents: Journal of Sedimentary Petrology, v. 52, p. 279–298.

Lowe, D.R., 1988, Suspended-load fallout rate as an independent variable in the analysis of current structures: Sedimentology, v. 35, p. 765-776.

Macauley, R.V., and Hubbard, S.M., 2013, Slope channel sedimentary processes and stratigraphic stacking, Cretaceous Tres Pasos Formation slope system, Chilean Patagonia: Marine and Petroleum Geology, v. 41, p. 146–162, doi: 10.1016/j.marpetgeo.2012.02.004.

Macdonald, H.A., Wynn, R.B., Huvenne, V.A., Peakall, J., Masson, D.G., Weaver, P.P., and McPhail, S.D., 2011a, New insights into the morphology, fill, and remarkable longevity (> 0.2 m.y.) of modern deep-water erosional scours along the northeast Atlantic margin: Geosphere, v. 7, p. 845–86, doi: 10.1130/GES00611.1.

Macdonald, H.A., Peakall, J., Wignall, P.B., and Best, J., 2011b, Sedimentation in deep-sea lobe-elements: implications for the origin of thickening-upward sequences: Journal of the Geological Society of London, v. 168, p. 319–331, doi: 10.1144/0016-76492010-036.

Marini, M., Milli, S., Ravnås, R., and Moscatelli, M., 2015, A comparative study of confined vs. semi-confined turbidite lobes from the Lower Messinian Laga Basin (Central Apennines, Italy): Implications for assessment of reservoir architecture: Marine and Petroleum Geology, v. 63, p. 142-165, doi: 10.1016/j.marpetgeo.2015.02.015.

Meckel III, L.D., Ugueto, G.A., Lynch, D.H., Hewett, B.M., Bocage, E.J., Winker, C.D., and O'Neill, B.J., 2002, Genetic stratigraphy, stratigraphic architecture, and reservoir stacking patterns of the upper Miocene–lower Pliocene greater Mars-Ursa intraslope basin, Mississippi Canyon, Gulf of Mexico, *in* Armentrout, J.M., and Rosen, N.C., eds., Sequence Stratigraphic Models for Exploration and Production: Evolving Methodology, Emerging Models, and Application Histories: GCSSEPM (Gulf Coast Section, Society for Sedimentary Geology) Foundation 22nd Annual Bob F. Perkins Research Conference Proceedings, p. 113-147.

Morris, S.A., Kenyon, N.H., Limonov, A.F., and Alexander, J., 1998, Downstream changes of large-scale bedforms in turbidites around the Valencia channel mouth, north-west Mediterranean: implications for palaeoflow reconstruction: Sedimentology, v. 42, p. 365-377, doi: 10.1046/j.1365-3091.1998.0160f.x.

Morris, E.A., Hodgson, D.M., Brunt, R.L., and Flint, S.S., 2014, Origin, evolution and anatomy of silt-prone submarine external levees: Sedimentology, v. 61, p. 1734-1763, doi:10.1111/sed.12114.

Mulder, T., and Alexander, J., 2001, Abrupt change in slope causes variation in the deposit thickness of concentrated particle-driven density currents: Marine Geology, v. 175, p. 221-235, doi: 10.1016/S0025-3227(01)00114-1.

Mutti, E., 1985, Systems and their relations to depositional sequences, *in* Zuffa, G.G., ed., Provenance of arenites: Interpreting provenance relations from detrital modes of sandstones: NATO-ASI Series 148: Dordrecht, D. Reidel, p. 65–93.

Mutti, E., 1992, Turbidite sandstones. Agip, Istituto di geologia, Università di Parma, Italy, p. 275.

Mutti, E., and Normark, W.R., 1987, Comparing examples of modern and ancient turbidite systems: problems and concepts, *in* Leggett, J.K., and Zuffa, G.G., eds., Marine Clastic Sedimentology: Concepts and Case Studies: Oxford, UK, Graham & Trotman, p. 1-38.

Mutti, E., and Normark, W.R., 1991, An integrated approach to the study of turbidite systems, *in* Weimer, P., and Link, M.H., eds., Seismic facies and sedimentary processes of submarine fans and turbidite systems: New York, Springer-Verlag, p. 75–106, doi: 10.1007/978-1-4684-8276-8_4.

Normark, W.R., and Piper, D.J.W., 1991, Initiation processes and flow evolution of turbidity currents: implications for the depositional record, *in* Osborne, R.H., ed., From Shoreline to Abyss: Contributions in Marine Geology in Honor of Francis Parker Shepard, Special publication- Society for Sedimentary Geology, v. 46, p. 207-230.

Normark, W.R., Piper, D.J.W., and Hess, G.R., 1979, Distributary channels, sand lobes, and mesotopography of Navy submarine fan, California Borderland, with applications to ancient fan sediments: Sedimentology, v. 26, p. 749-774.

O'Byrne, C.J., Prather, B.E., Steffens, G.S., and Pirmez, C., 2004, Reservoir architectural styles across stepped slope profiles: Implications for exploration, appraisal and development: American Association of Petroleum Geologists, International Conference and Exhibition, Cancún, Mexico, Abstracts CD.

Palanques, A., Kenyon, N.H., Alonso, B., and Limonov, A.F., 1995, Erosional and depositional patterns in the Valencia Channel Mouth: an example of a modern channel-lobe transition zone: Marine Geophysical Research, v. 18, p. 103-118, doi: 10.1007/BF01204341.

Peakall, J., McCaffrey, W.D., and Kneller, B.C., 2000, A process model for the evolution, morphology, and architecture of sinuous submarine channels: Journal of Sedimentary Research, v. 70, p. 434–448.

Pemberton, E.A.L., Hubbard, S.M., Fildani, A., Romans, B., and Stright, L., 2016, The stratigraphic expression of decreasing confinement along a deep-water sediment routing system: Outcrop example from southern Chile: Geosphere, v. 12, p. 114-134, doi: 10.1130 /GES01233.1.

Piper, D. J. W., and Normark, W. R., 1983, Turbidite depositional patterns and flow characteristics, Navy submarine fan, California borderland: Sedimentology, v. 30, p. 681–694. Piper, D.J.W., and Deptuck, M., 1997, Fine grained turbidites of the Amazon Fan: facies characterization and interpretation, *in* Flood, R.D., Piper, D.J.W., Klaus, A., Peterson, L.C. eds., Proceedings of the Ocean Drilling Program: Scientific Results, v. 155, p. 79-108

Pirmez, C., Beaubouef, R.T., Friedmann, S.J. and Mohrig, D.C., 2000, Equilibrium profile and base level in submarine channels: examples from Late Pleistocene systems and implications for the architecture of deep-water reservoirs, *in* Weimer, P., Slatt, R.M., et al. eds., Deep-water Reservoirs of the World: Gulf Coast Society of the Society of Economic Paleontologists and Mineralogists Foundation, 20th Annual Research Conference, p. 782–805.

Plink-Björklund, P., and Steel, R., 2002, Sea-level fall below the shelf edge, without basin-floor fans: Geology, v. 30, p. 115–118.

Postma, G., Hoyal, D.C., Abreu, V., Cartigny, M.J., Demko, T., Fedele, J.J., Kleverlaan, K., and Pederson, K.H., 2016, Morphodynamics of supercritical turbidity currents in the channel-lobe transition zone, *in* Lamarche, G., Mountjoy, J., Bull, S., Hubble, T., Krastel, S., Lane, E., Micallef, A., Moscardelli, L., Mueller, C., Pecher, I., and Woelz, S. eds., Submarine Mass Movements and Their Consequences: 7th International Symposium, Springer International Publishing, p. 469-478.

Prather, B.E., 2003, Controls on reservoir distribution, architecture and stratigraphic trapping in slope settings: Marine and Petroleum Geology, v. 20, p. 529-545, doi: 10.1016/j.marpetgeo.2003.03.009.

Prather, B.E., Pirmez, C., Sylvester, Z. and Prather, D.S., 2012, Stratigraphic response to evolving geomorphology in a submarine apron perched on the upper Niger delta slope, *in* Prather, B.E., Deptuck, M.E., Mohrig, D., van Hoorn, B., and Wynn, R.B. eds., Application of the Principles of Seismic Geomorphology to Continental-Slope and Base-of-Slope Systems: Case Studies From Seafloor and Near-Seafloor Analogues. SEPM Special Publication 99, p. 145–161.Prather, B.E., O'Byrne, C., Pirmez, C., and Sylvester, Z., 2017, Sediment partitioning, continental slopes and base-of-slope systems: Basin Research, v. 29, p. 394-416, doi: 10.1111/bre.12190.

Prélat, A., and Hodgson, D.M., 2013, The full range of turbidite bed thickness patterns in submarine lobes: Controls and implications: Journal of the Geological Society, v. 170, p. 209-214, doi: 10.1144/jgs2012-056.

Prélat, A., Hodgson, D.M., and Flint, S.S., 2009, Evolution, architecture and hierarchy of distributary deep-water deposits: a high-resolution outcrop investigation from the Permian Karoo Basin, South Africa: Sedimentology, v. 56, p. 2132-2154, doi: 10.1111/j.1365-3091.2009.01073.x.

Prélat, A., Covault, J.A., Hodgson, D.M., Fildani, A. and Flint, S.S., 2010, Intrinsic controls on the range of volumes, morphologies, and dimensions of submarine lobe: Sedimentary Geology, v. 232, p.66-76.

Pyles, D.R., Strachan, L.J. and Jennette, D.C., 2014, Lateral juxtapositions of channel and lobe elements in distributive submarine fans: Three-dimensional outcrop study of the Ross Sandstone and geometric model: Geosphere, v. 10, p.1104-1122.

Sinclair, H.D., and Tomasso, M., 2002, Depositional evolution of confined turbidite basins: Journal of Sedimentary Research, v. 72, p. 451-456, doi: 10.1306/111501720451.

Smith, R., 2004a, Turbidite systems influenced by structurally induced topography in the multi-sourced Welsh Basin, *in* Lomas, S.A., and Joseph, P., eds., Confined Turbidite Systems: Geological Society of London Special Publication 222, p. 209-228.

Smith, R., 2004b, Silled sub-basins to connected tortuous corridors: Sediment distribution systems on topographically complex sub-aqueous slopes, *in* Lomas, S.A., and Joseph, P., eds., Confined Turbidite Systems: Geological Society of London Special Publication 222, p. 23–43, doi: 10.1144/GSL.SP.2004.222.01.03.

Spikings, A.L., Hodgson, D.M., Paton, D.A., and Spychala, Y.T., 2015, Palinspastic restoration of an exhumed deepwater system: A workflow to improve paleogeographic reconstructions: Interpretation, v. 3, p. SAA71-SAA87, doi: 10.1190/INT-2015-0015.1.

Spychala, Y.T., Hodgson, D.M., Flint, S.S., and Mountney, N.P., 2015, Constraining the sedimentology and stratigraphy of submarine intraslope lobe deposits using exhumed examples from the Karoo Basin, South Africa: Sedimentary Geology, v. 322, p. 67-81, doi: 10.1016/j.sedgeo.2015.03.013.

Spychala, Y.T., Hodgson, D.M., Stevenson, C.J., and Flint, S.S., 2017, Aggradational lobe fringes: The influence of subtle intrabasinal seabed topography on sediment gravity flow processes and lobe stacking patterns: Sedimentology, v. 64, p. 582-608.

Stevenson, C.J., Jackson, C.A-L., Hodgson, D.M., Hubbard, S.M., and Eggenhuisen, J., 2015, Sediment bypass in deep-water systems: Journal of Sedimentary Research, v. 85, p. 1058-1081, doi: 10.2110/jsr.2015.63.

Stow, D.A., and Johansson, M., 2002, Deep-water massive sands: nature, origin and hydrocarbon implications: Marine and Petroleum Geology, v. 17, p. 145-174, doi:10.1016/S0264-8172(99)00051-3.

Sumner, E.J., Amy, L.A., and Talling, P.J., 2008, Deposit structure and process of sand deposition from decelerating sediment suspensions: Journal of Sedimentary Research, v. 78, p. 529-547, doi: 10.2110/jsr.2008.062.

Sumner, E.J., Peakall, J., Parsons, D.R., Wynn, R.B., Darby, S.E., Dorrell, R.M., McPhail, S.D., Perrett, J., Webb, A., and White, D., 2013, First direct measurements of hydraulic jumps in an active submarine density current: Geophysical Research Letters, v. 40, p. 5904-5908, doi: 10.1002/2013GL057862.

Symons, W.O., Sumner, E.J., Talling, P.J., Cartigny, M.J., and Clare, M.A., 2016, Large-scale sediment waves and scours on the modern seafloor and their implications for the prevalence of supercritical flows: Marine Geology, v. 371, p. 130–148, doi: 10.1016/j.margeo.2015.11.009.

Talling, P.J., 2013, Hybrid submarine flows comprising turbidity current and cohesive debris flow: Deposits, theoretical and experimental analyses, and generalized models: Geosphere, v. 9, p. 460-488, doi: 10.1130/GES00793.1.

Talling, P.J., Amy, L.A., Wynn, R.B., Peakall, J., and Robinson, M., 2004, Beds comprising debrite sandwiched within co-genetic turbidite: origin and widespread occurrence in distal depositional environments: Sedimentology, v. 51, p. 163-194, doi: 10.1111/j.1365-3091.2004.00617.x.

Talling, P.J., Masson, D.G., Sumner, E.J., and Malgesini, G., 2012, Subaqueous sediment density flows: Depositional processes and deposit types: Sedimentology, v. 59, p. 1937-2003, doi: 10.1111/j.1365-3091.2012.01353.x.

Tankard, A., Welsink, H., Aukes, P., Newton, R., and Stettler, E., 2009, Tectonic evolution of the Cape and Karoo basins of South Africa: Marine and Petroleum Geology, v. 26, p. 1379-1412, doi: 10.1111/j.1365-3091.2012.01353.x.

Tankard, A., Welsink, H., Aukes, P., Newton, R., and Stettler, E., 2012**,** Chapter 23: Geodynamic interpretation of the Cape and Karoo basins, South Africa, *in* Rioberts, D.G., and Bally, A.W., eds., Phanerozoic Passive Margins, Cratonic Basins and Global Tectonic Maps: Amsterdam, Elsevier, p. 869-94.

van der Merwe, W., Flint, S., and Hodgson, D., 2010, Sequence stratigraphy of an argillaceous, deepwater basin plain succession: Vischkuil Formation (Permian), Karoo Basin, South Africa: Marine and Petroleum Geology, v. 27, p. 321-333, doi: 10.1016/j.marpetgeo.2009.10.007.

van der Merwe, W., Flint, S., and Hodgson, D., 2014, Depositional architecture of sand-attached and sand-detached channel-lobe transition zones on an exhumed stepped slope mapped over a 2500 km2 area: Geosphere, v. 10, p. 1076-1093, doi: 10.1130/GES01035.1.

Vicente Bravo, J.C., and Robles, S., 1995, Large-scale mesotopographic bedforms from the Albion Black Flysch, northern Spain: characterization, setting and comparison with recent analogues, *in* Pickering, K.T., Hiscott, R.N., Kenyon, N.H., Ricci Lucchi, F., and Smith, R.D.A., eds., Atlas of Deep Water Environments: Architectural Style in Turbidite Systems: London, Chapman and Hall, p. 216–226, doi: 10.1007/978-94-011-1234-5_32.

Visser, J.N.J., 1997, Deglaciation sequences in the Permo-Carboniferous Karoo and Kalahari basins of the southern Africa: a toll in the analysis of cyclic glaciomarine basin fills: Sedimentology, v. 44, p. 507–521, doi: 10.1046/j.1365-3091.1997.d01-35.x.

Visser, J.N.J., and Prackelt, H.E., 1996, Subduction, mega-shear systems and Late Palaeozoic basin development in the African segment of Gondwana: Geologische Rundschau, v. 85, p. 632–646, doi: 10.1007/BF02440101.

Vrolijk, P.J., and Southard, J.B., 1997, Experiments on rapid deposition of sand from high-velocity flows: Geoscience Canada, v. 24, p. 45-54.

Waltham, D., 2004, Flow transformations in particulate gravity currents: Journal of Sedimentary Research, v. 74, p. 129–134, doi: 10.1306/062303740129.

Weirich, F., 1989, The generation of turbidity currents by subaerial debris flows, California: Geological Society of America Bulletin, v. 101, p. 278-291.

Wynn, R.B., and Stow, D.A., 2002, Classification and characterisation of deep-water sediment waves: Marine Geology, v. 192, p. 7-22, doi: 10.1016/S0025-3227(02)00547-9.

Wynn, R.B., Kenyon, N.H., Masson, D.G., Stow, D.A., and Weaver, P.P., 2002a, Characterization and recognition of deep-water channel-lobe transition zones: AAPG Bulletin, v. 86, p. 1441–1446.

Wynn, R.B., Piper, D.J.W., and Gee, M.J.R., 2002b, Generation and migration of coarse-grained sediment waves in turbidity current channels and channel–lobe transition zones: Marine Geology, v. 192, p. 59-78, doi: 10.1016/S0025-3227(02)00549-2.

Captions

Figure 1- (A) Location of the study area within southwestern Africa. Black box indicates location of map B. (B) Regional geological map of the Western Cape. The study area is located in the Laingsburg depocenter, where Ecca Group stratigraphy is exposed, north of the Swartberg branch of the Cape Fold Belt (Modified from Flint et al., 2011).

Figure 2- (A) Stratigraphic column showing the Permian Ecca Group deposits in the Laingsburg depocenter, southwestern Karoo Basin. This stratigraphy represents margin progradation from deepwater basin plain deposits (Vischkuil and Laingsburg formations), through submarine slope (Fort Brown Formation) and continues to shallow water (Waterford Formation). Blue box indicates detailed section shown in B. (B) Submarine slope system Unit D/E and Unit E of the Fort Brown Fm., the focus of this study (modified from van der Merwe et al., 2014).

Figure 3- (A) Location of the study area relative to Laingsburg town. Dashed lines indicate the location of outcrop belts. White shading indicates the exposure of Fort Brown and Laingsburg formations. Locations marked Roggekraal, Zoutkloof and Geelbek are the study areas related to the corresponding updip deposits of Unit E (Spychala et al., 2015). (B) Enlarged area shows the four sections of regional panels involved in this study and the key Slagtersfontein location. The northern panel 1, contains 64 logs, the central northern panel 2, contains 67 logs, the central southern panel 3, contains 39 logs, and the southern panel 4 contains 30 logs. The highest concentration of data is in the Slagtersfontein study area on panel 2. Locally the top of Unit E3 along panel 3 is lost to modern erosion by a tributary of the Gamka River. Aerial photographs are from NASA Visible Earth (National Aeronautics and Space Administration, http://visibleearth.nasa.gov/; regional scale) and Chief Directorate: National Geo-spatial Information, South Africa (http://www.ngi.gov.za/; Laingsburg depocenter). (C) Google Earth image of Slagtersfontein study area showing laterally continuous Unit D and abrupt thickening of Unit E downdip. Tops and bases of units are mapped by walking surfaces and tracking with GPS.

Figure 4- Regional dip correlation panel along the Baviaans South outcrop belt with data from previous studies (van der Merwe et al., 2014; Spychala et al., 2015), showing the D-E interunit mudstone, Unit D/E, Unit E, and the E-F interunit mudstone Interpretations of architectural elements show the downdip transition in Unit E from slope channels, through intraslope lobes, channel-levee systems and channel-lobe transition zone, to basin-floor fans. Datum used is top Unit B, an underlying basin-floor fan (shown in Fig. 2A). Map highlights the location of outcrop belt within Figure 3, with the red line denoting the location of this dip section and black dashed lines showing other exposed sections

Figure 5- Representative photographs of sedimentary facies. (A) Structureless sandstone; (B) Structured sandstone, dashed white lines indicate sheared climbing ripple laminations; (C) Mudstone clast conglomerate; (D) Scoured siltstone and sandstone, dashed red lines indicate erosional surfaces; (E) Hybrid beds, dashed white line indicates division between lower sandstone turbidite and upper debrite; (F) Interbedded sandstone and siltstone; (G) Remobilized deposits; (H) Hemipelagic mudstone. Scales: logging pole with 10 cm divisions, camera lens 7 cm in diameter.

Figure 6- Regional correlation panels of Unit D/E and subunits E2 and E3. Panels positioned north (top) to south (base). Southern panel (panel 4) shown on Figure 7 with architectural elements, consisting of E3 with two small outcrops of Unit E2, in the updip area. Relative spatial positions shown in fence diagram (Fig. 8). More detailed panel of Slagtersfontein CLTZ shown in figures 10 & 11. Rose diagrams show paleocurrent directions from ripples, grooves and flutes throughout all units.

Figure 7- Regional correlation panels showing architectural elements of Unit D/E and subunits E2 and E3. For Unit divisions of panels A, B and C see Figure 6. For logs and more detailed panels, see supplementary material.

Figure 8- Fence diagram showing 3D architecture and architectural elements of Units D/E, E2 and E3. For geographic positions of outcrop belts see Figure 3B. For unit divisions see Figure 6. For key see Figure 7.

Figure 9- Combined thickness isopach maps and gross depositional environment reconstructions for (A) Unit D/E, (B) Subunit E2 and (C) Subunit E3. Contours indicate thickness of unit in meters, contour spacing at 2 m for D/E, 1 m for E2 and 5 m for E3. Black circles indicate locations of data from logged sections shown on panels (Figs. 6 & 7), red circles indicate data from logs presented in supplementary information. White arrows indicate average paleocurrent direction. Geographic area covered is the same as that shown in Figure 3B, presented in palinspastically restored positions Mapped thickness distributions were created by fitting a surface to thickness values extracted from the logged sections. The surfacing operation was conducted in ArcGIS using the simple kriging tool within the Geostatistical Wizard (http://resources.arcgis.com/en/home/). Output maps are extended to the extremities of the input data by the surfacing algorithm, which creates rectangular maps that may extend beyond the edge of the input data. Additional modifications were made to subunit E3 surfaces to account for minimum values of the downdip logged sections along panel 3. Channel and lobe boundaries are not precise locations and are interpreted from thickness trends and paleocurrent directions. Paleogeographic maps are based on the distribution of sedimentary facies and architectural elements, and illustrate the gross depositional environment for the stratigraphic interval presented.

Figure 10- Slagtersfontein detailed section, location shown on figure 6, 7 and 8. Updip area of Slagtersfontein panel, divided into sections 1-3 for description purposes. Deposits transition from levee (section 1) to sediment bypass dominated zone (sections 2 & 3), figure 11 continues downdip showing sections 4 and 5. (A) Simplified panel section across whole Slagtersfontein study area, highlighting the focus of this figure. Colors indicate subunits E2 and E3 separated by the E2-E3 intra-unit mudtone. (B) Panel showing logged sections of E2 and E3, datumed on Top Unit D. For larger regional panel 2, see figures 7 and 8. Logs and log key are in supplementary material. (C) Schematic sketch of key features in subunits E2 and E3 across section, showing downdip changes in thickness, facies and sedimentary structures.

Figure 11- Downdip area of Slagtersfontein panel, continuing from Figure 10, divided into sections 4-5 for description purposes. Deposits transition from thin, dewatered, scoured and reworked sandstone (section 4) to abruptly thickening lobe deposits (section 5). (A) Simplified panel section across whole Slagtersfontein study area, highlighting the focus of this figure. Colors indicate sub-units E2 and E3 separated by the E2-E3 intra-unit mudstone. (B) Panel showing logged sections of E2 and E3, and localized deposition of Unit D/E. Datum for panel is Top Unit D and logs are in supplementary material. (C) Schematic sketch of key features in subunits E2 and E3 showing downdip changes in thickness, facies and sedimentary structures.T1- T4 refer to sequence of deposition shown in Figure 15. For key see Figure 10.

Figure 12- Representative photographs of Unit E3 over sections 2 to 5 of the Slagtersfontein CLTZ. (A) Basal spill-over fringe deposits and aggradational sandstone bed. (B) Composite erosional surfaces, aggradational sandstone bed with scoured top and overlying siltstone and lag deposits. (C) Rippled thin sandstone beds. (D) Discontinuous lenticular sandstone beds cut by erosional surfaces and draped by lags. (E) Highly dewatered sandstone beds with erosional surfaces throughout. (F) Megaflute scour at top of unit, eroding dewatered sandstone. (G) Thin eroded sandstone bed, constituting the entire coarse component of E3. (H) Thick amalgamated sandstone beds and sand-rich hybrid beds of E3 proximal lobes. (I) Discontinuous lenticular sandstone beds, cut by erosional surfaces and draped by lags, at the base of E3 lobe deposits. (J) Sand-rich hybrid bed. Scales: logging pole with 10 cm divisions, notebook 15 cm in length.

Figure 13- (A) Location of section shown in B and C within the CLTZ. Colors indicate subunits E2 and E3 separated by the E2-E3 intra-unit mudstone. (B) Outline of beds over outcrop and colored with architectural elements scheme. Abbreviations: Sc. st. & sd.- Scoured siltstone and sandstone, Int. st. & sd.- Interbedded siltstone and sandstone, Lag- Bypass lag, St-less sand- Structureless sandstone, Int. st. & sd.- Interbedded siltstone and sandstone, E2-E3 st.- E2- E3 intra-unit mudstone , Int. silt.- Interbedded siltstone, SOF- Spill-over fringe, D-E silt- Unit D-E inter-unit mudstone. (B) Sections logged at mm scale over 20 m outcrop distance, showing bed scale changes in subunits E2 and E3 within the CLTZ. This key area shows features consistent with a fluctuation of high and low energy deposits throughout E3, with a layering of medium sandstone, low energy thin-beds, composite erosional surface with mudclast lags, thick aggradational beds, and further erosional surface and lag deposits which decrease upwards. For whole Slagtersfontein section see Figures 10 and 11.

Figure 14- Summary figure of overall stepped-slope profile architecture and related deposits of Unit E. Flows were fed through entrenched slope channels to intraslope lobes, and channel levee systems, to the CLTZ and basin-floor lobes. Logs show typical section through key areas. Logs from outside of the study area modified from van der Merwe et al., 2014.

Figure 15- Sketch of interpreted variations in the CLTZ over the Slagtersfontein section shown in Figures 10 and 11. T1-T4 show the minimum extent of progressive expansions and contractions of the CLTZ. T1 shows the initial location of bypass and deposition dominated areas with initial deposition of structured sandstone with a minimum thickness of a few meters. T2 shows the eastward movement or extension of the bypass dominated channel-lobe transition zone, with erosion of initial lobe deposits and focus of deposition shifted downdip. T3 shows the westward movement or contraction of the bypass zone and backfilling of the system, with build-up of sand-rich proximal lobe deposits over bypass surfaces. T4 shows the final stage of CLTZ extension or easterly movement, indicated by efficient sediment bypass in the updip area, a large erosional surface cutting into the lobes and a widespread megaflute surface which expands downdip of this area.

Figure 16- (A) Plan view of a CLTZ, highlighting the key depositional features and their spatial distribution modified from Wynn et al. (2002). Note area of mixed depositional and erosional features, area of reworked and scoured lobe and axial- and off-axis proximal lobe deposits. Diagram in Wheeler space illustrates movement of a CLTZ over 6 time periods A-F,

with (B) showing a plan view outline for each time period and (C) illustrating resultant build-up of deposits and potential erosion over a dip-section (X-X') and a distal strike-section. (D) A further strike-section through a more proximal area of the CLTZ, illustrating deposition and potential erosion. This diagram highlights the composite nature of deposits and erosional surfaces throughout CLTZs and the dynamic expansions, contractions and shifting of the zone that they represent. Overall preservation potential is variable but low, with shifting of the zone often decimating evidence of previous positions. The dark black lines represent periods of migration of the CLTZ. Gray draping units represent a hiatus in sand deposition and may include silt-rich lateral or frontal lobe fringe.

Table 1- Facies groups

Table 2- CLTZ lengths from modern sea-floor datasets (modified from Wynn et al., 2002).

Table 3- Key characteristics of CLTZ model with examples from other outcrop and modern seabed studies.

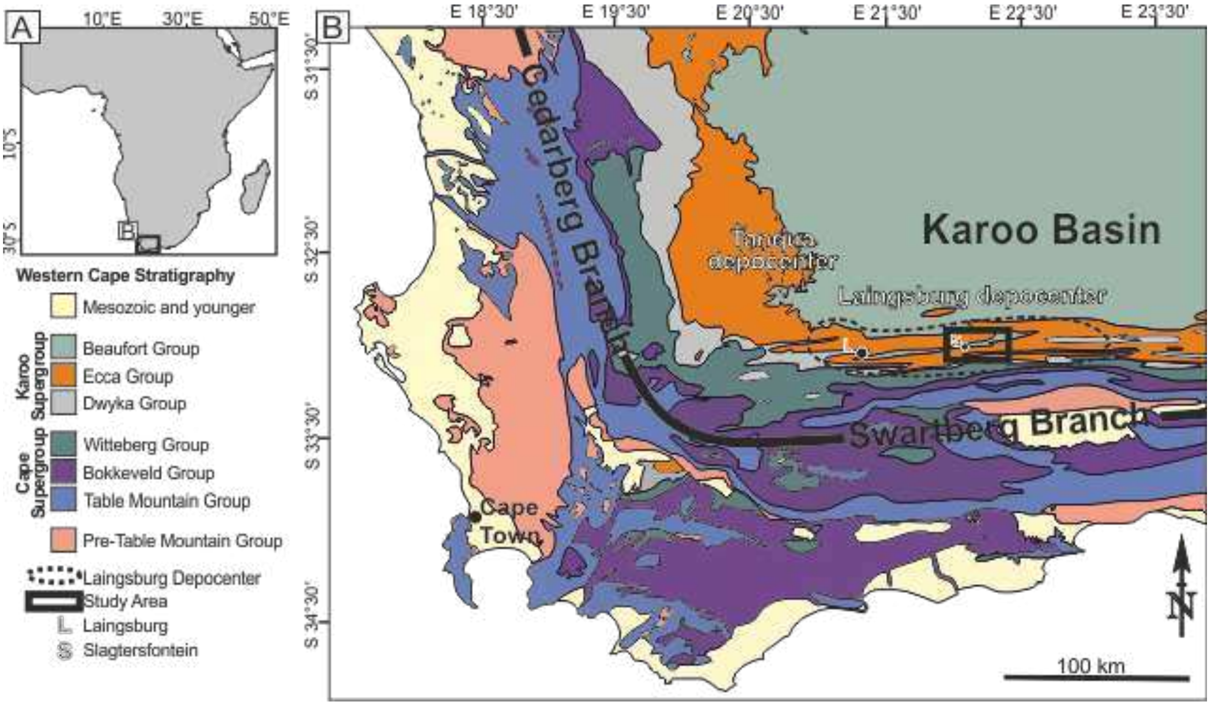
A
10°E
30°E
50°E
10°S
30°S
B
Western Cape Stratigraphy
Mesozoic and younger
Karoo Supergroup
Beaufort Group
Ecca Group
Dwyka Group
Cape Supergroup
Witteberg Group
Bokkeveld Group
Table Mountain Group
Pre-Table Mountain Group
Laingsburg Depocenter
Study Area
Laingsburg
Slagtersfontein
E 18°30'
E 19°30'
E 20°30'
E 21°30'
E 22°30'
E 23°30'
S 31°30'
S 32°30'
S 33°30'
S 34°30'
Karoo Basin
Tanqua depocenter
Laingsburg depocenter
Cedarberg Branch
Swartberg Branch
Cape Town
N
100 km

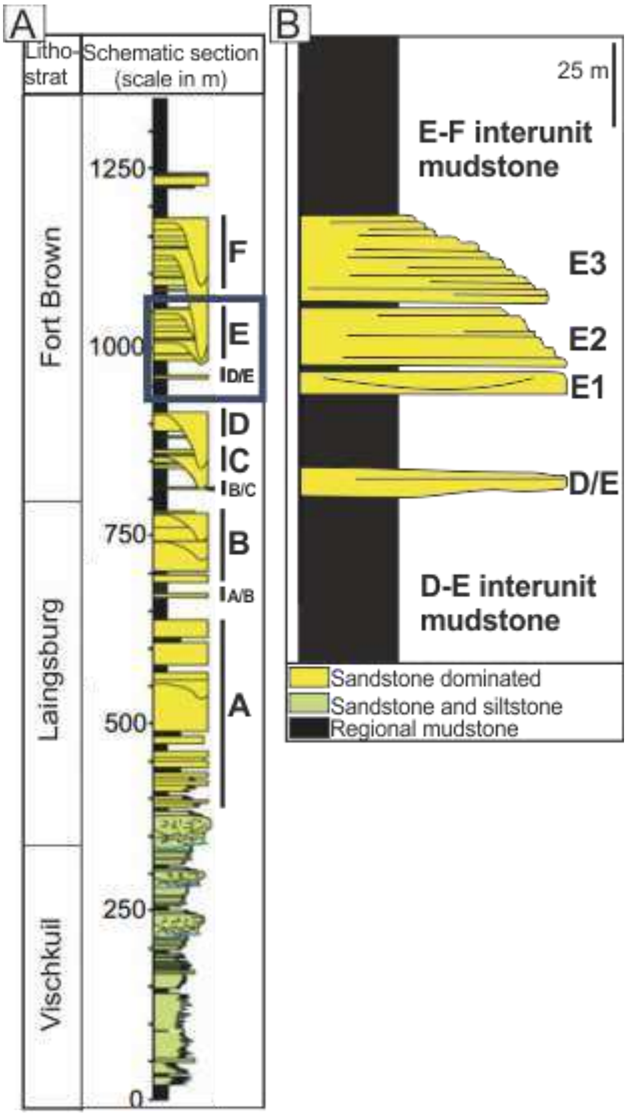
A
Litho-strat
Schematic section (scale in m)
Fort Brown
Laingsburg
Vischkuil
1250
1000
750
500
250
0
F
E
D/E
D
C
B/C
B
A/B
A
B
25 m
E-F interunit mudstone
E3
E2
E1
D/E
D-E interunit mudstone
Sandstone dominated
Sandstone and siltstone
Regional mudstone

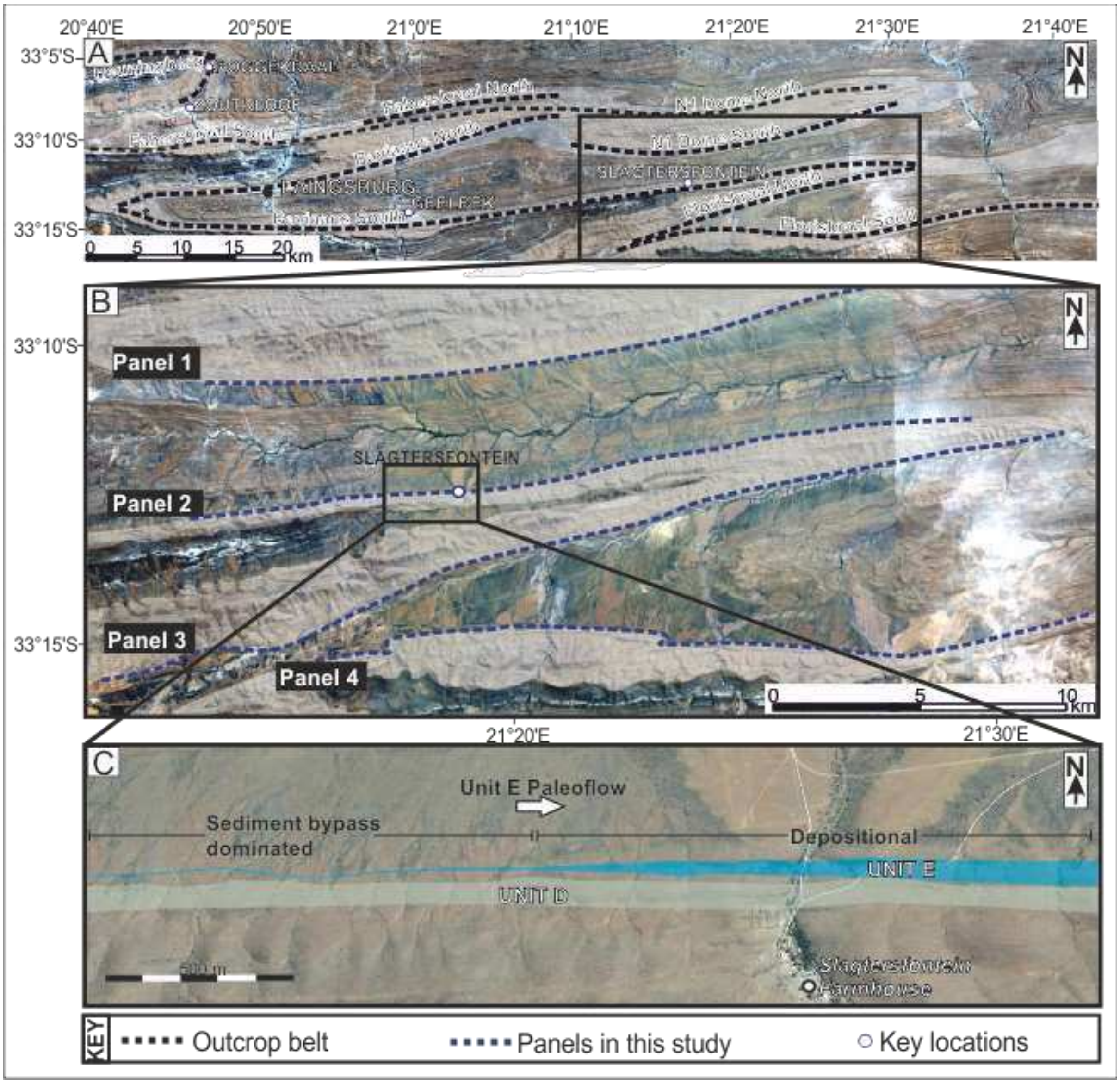

20°40'E
20°50'E
21°0'E
21°10'E
21°20'E
21°30'E
21°40'E
33°5'S
33°10'S
33°15'S
A
B
C
N
0 5 10 15 20 km
Panel 1
Panel 2
Panel 3
Panel 4
SLAGTERSFONTEIN
0 5 10 km
21°20'E
21°30'E
Unit E Paleoflow
Sediment bypass dominated
Depositional
UNIT E
UNIT D
Slagtersfontein Farmhouse
KEY
Outcrop belt
Panels in this study
Key locations

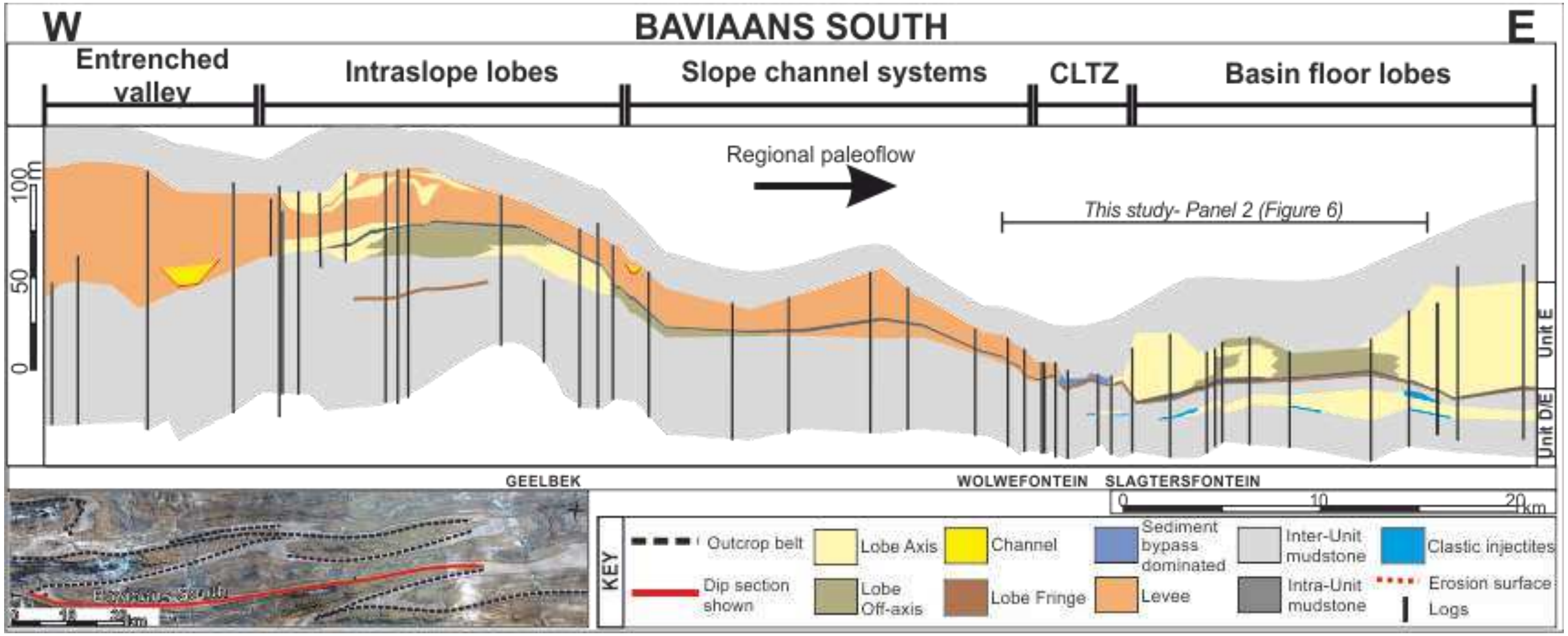

W
BAVIAANS SOUTH
E
Entrenched valley
Intraslope lobes
Slope channel systems
CLTZ
Basin floor lobes
Regional paleoflow
This study- Panel 2 (Figure 6)
100m
50
0
Unit E
Unit D/E
GEELBEK
WOLWEFONTEIN
SLAGTERSFONTEIN
0
10
20km
KEY
Outcrop belt
Dip section shown
Lobe Axis
Lobe Off-axis
Channel
Lobe Fringe
Sediment bypass dominated
Levee
Inter-Unit mudstone
Intra-Unit mudstone
Clastic injectites
Erosion surface
Logs

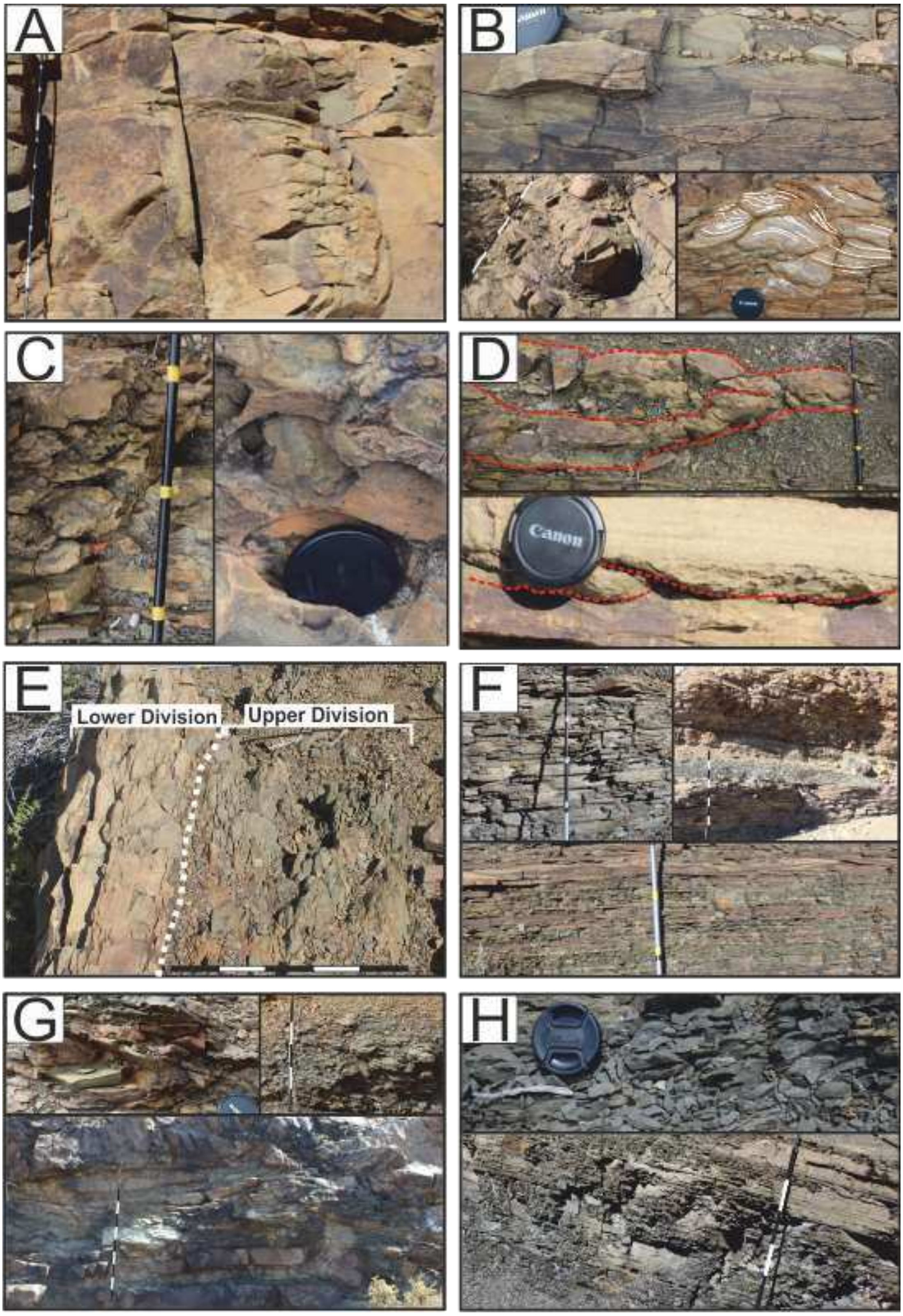

1272

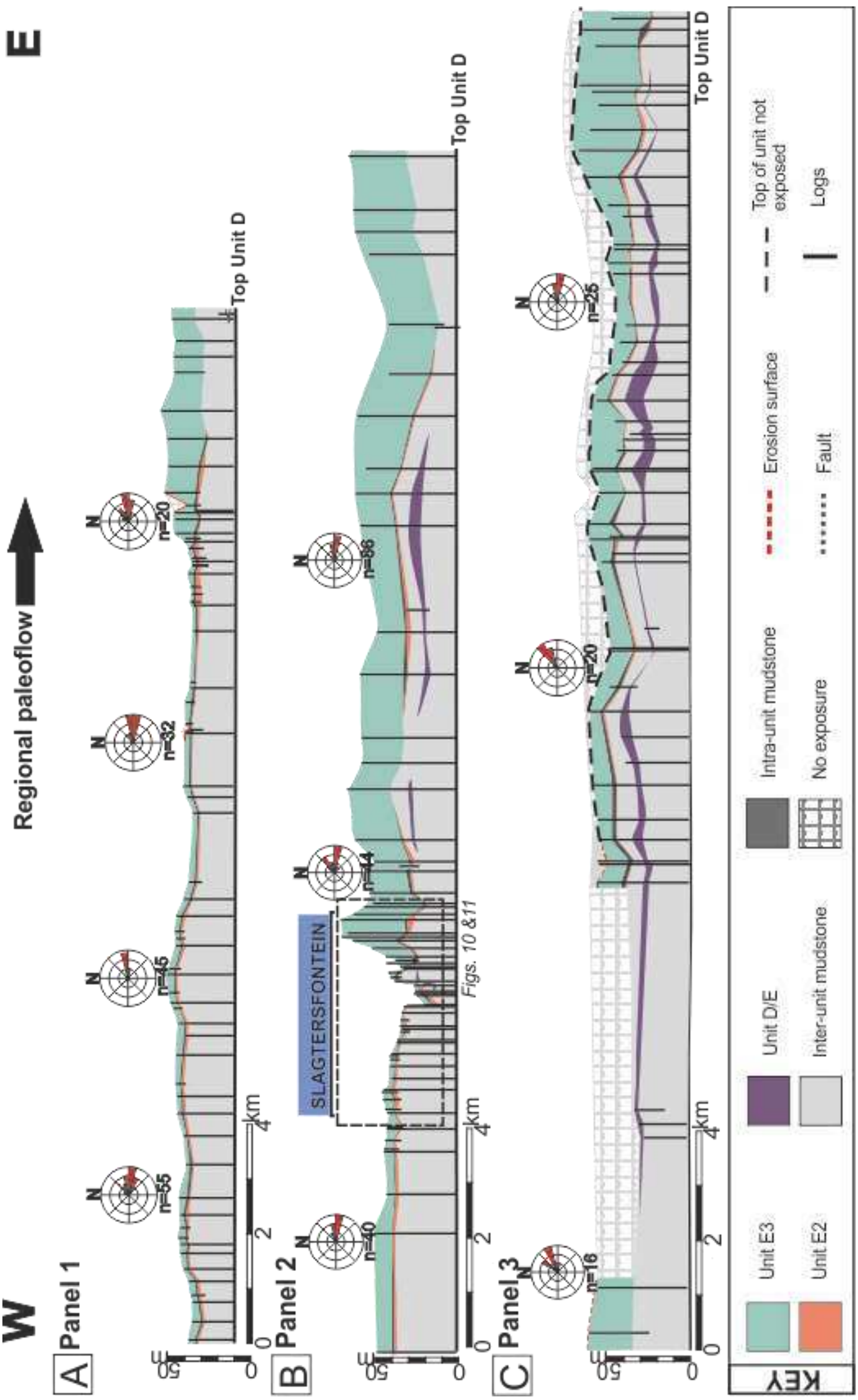

W
E
Regional paleoflow
A
Panel 1
B
Panel 2
C
Panel 3
Top Unit D
SLAGTERSFONTEIN
Figs. 10 &11
n=55
n=45
n=32
n=20
n=40
n=44
n=36
n=16
n=20
n=25
N
50
0
m
0
2
4
km
KEY
Unit E3
Unit E2
Unit D/E
Inter-unit mudstone
Intra-unit mudstone
No exposure
Erosion surface
Fault
Top of unit not exposed
Logs

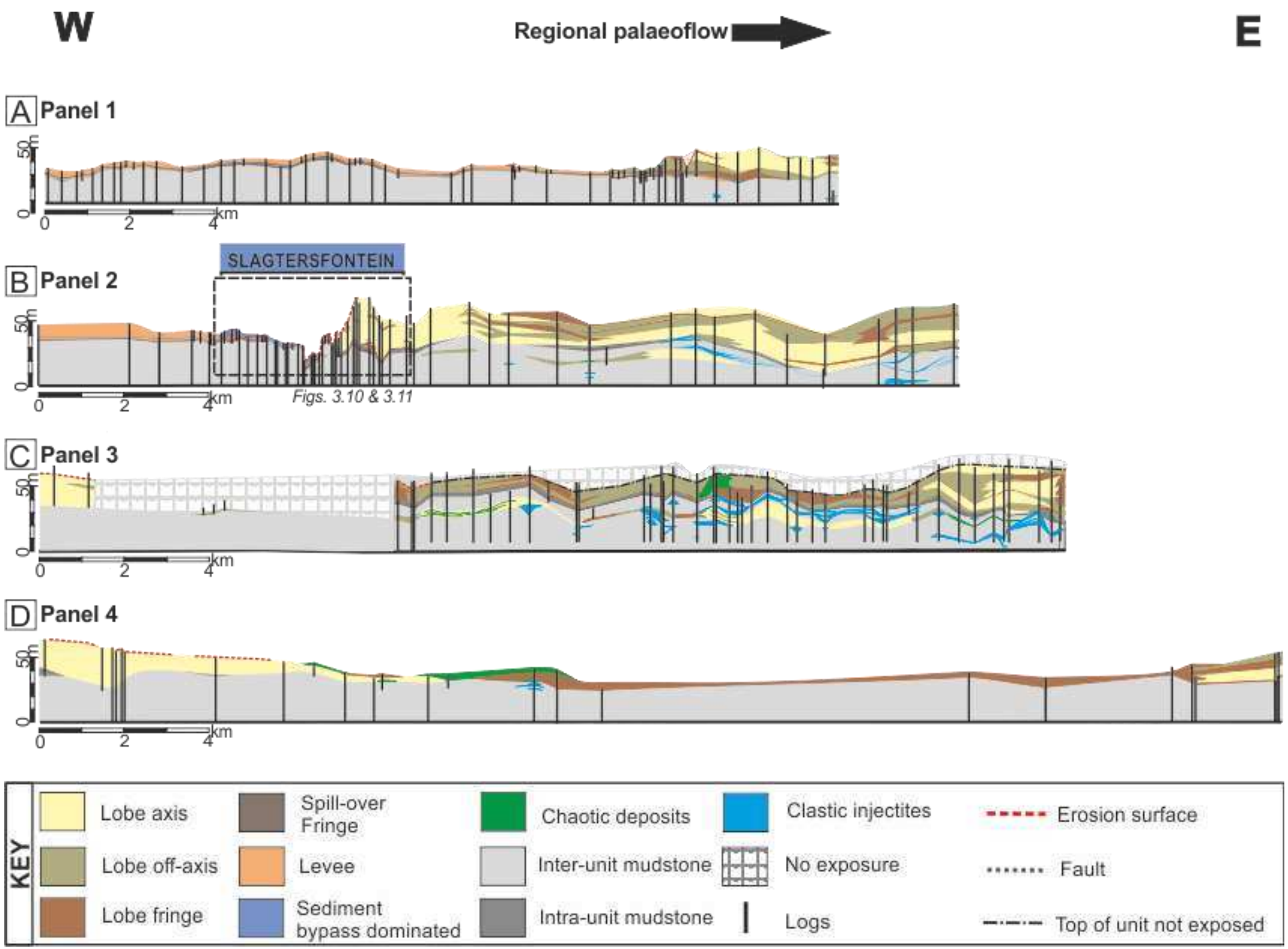
W
Regional palaeoflow
E
A Panel 1
50m
0
0
2
4km
SLAGTERSFONTEIN
B Panel 2
50m
0
0
2
4km
Figs. 3.10 & 3.11
C Panel 3
50m
0
0
2
4km
D Panel 4
50m
0
0
2
4km
KEY
Lobe axis
Lobe off-axis
Lobe fringe
Spill-over Fringe
Levee
Sediment bypass dominated
Chaotic deposits
Inter-unit mudstone
Intra-unit mudstone
Clastic injectites
No exposure
Logs
Erosion surface
Fault
Top of unit not exposed

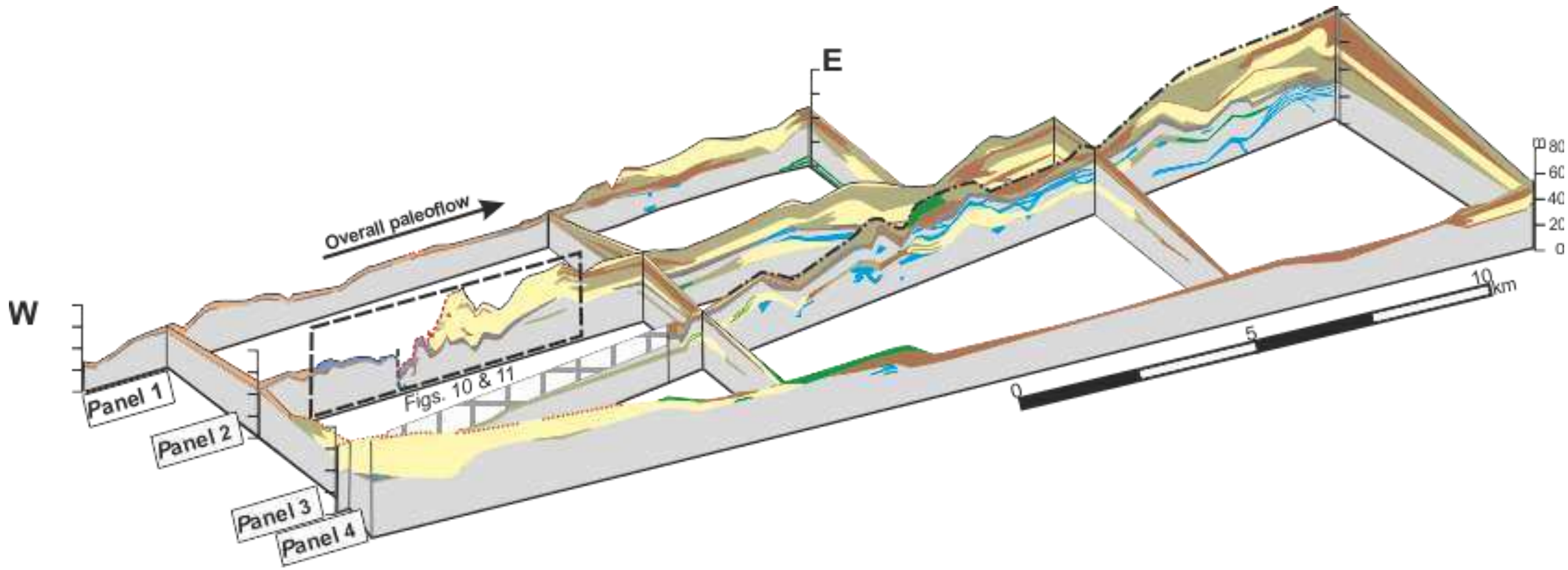
W
E
Overall paleoflow
Figs. 10 & 11
Panel 1
Panel 2
Panel 3
Panel 4
0
5
10
km
m
80
60
40
20
0

1276

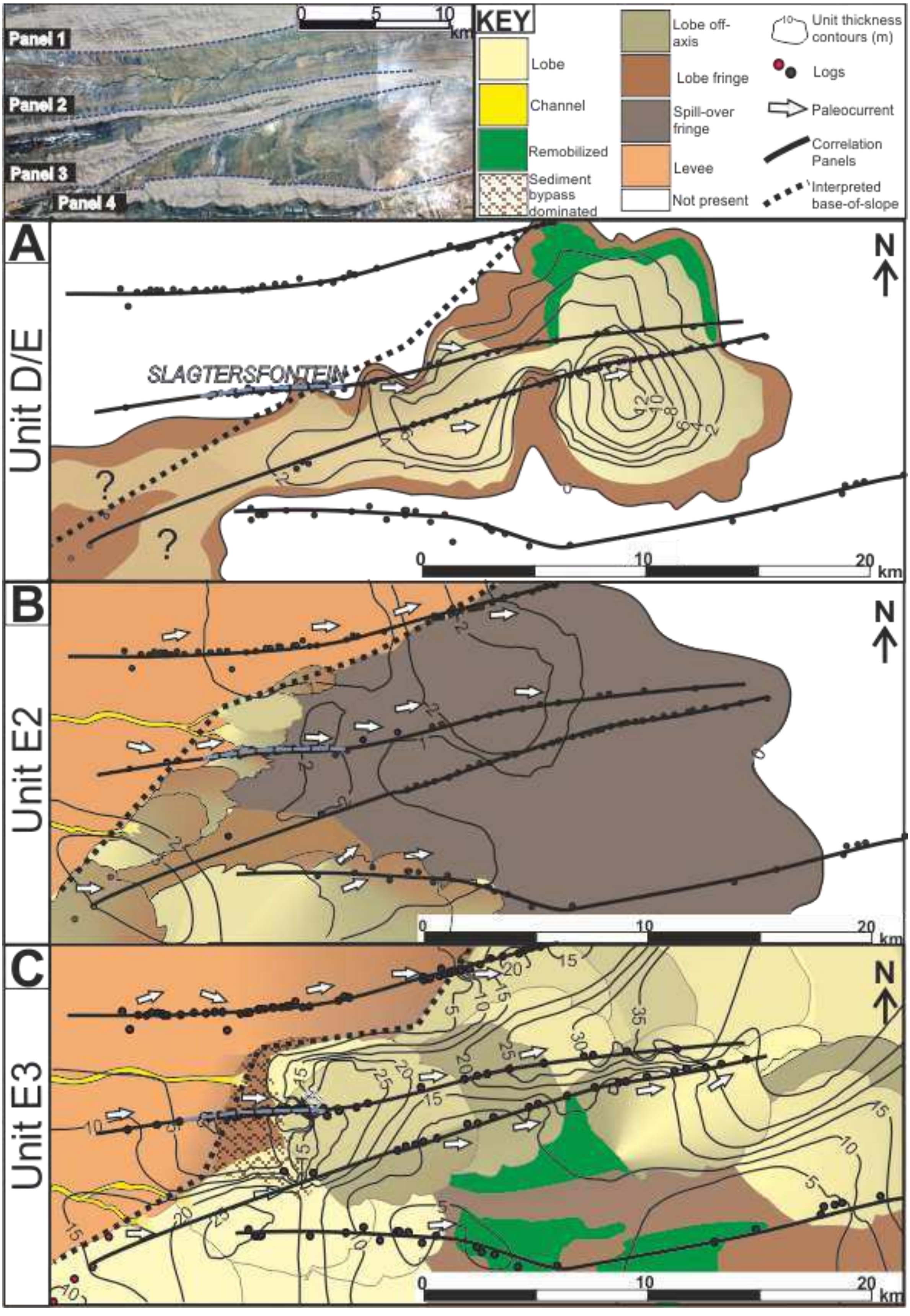

Panel 1
Panel 2
Panel 3
Panel 4
0 5 10 km
KEY
Lobe
Channel
Remobilized
Sediment bypass dominated
Lobe off-axis
Lobe fringe
Spill-over fringe
Levee
Not present
Unit thickness contours (m)
Logs
Paleocurrent
Correlation Panels
Interpreted base-of-slope
A
Unit D/E
SLAGTERSFONTEIN
N
0 10 20 km
B
Unit E2
C
Unit E3

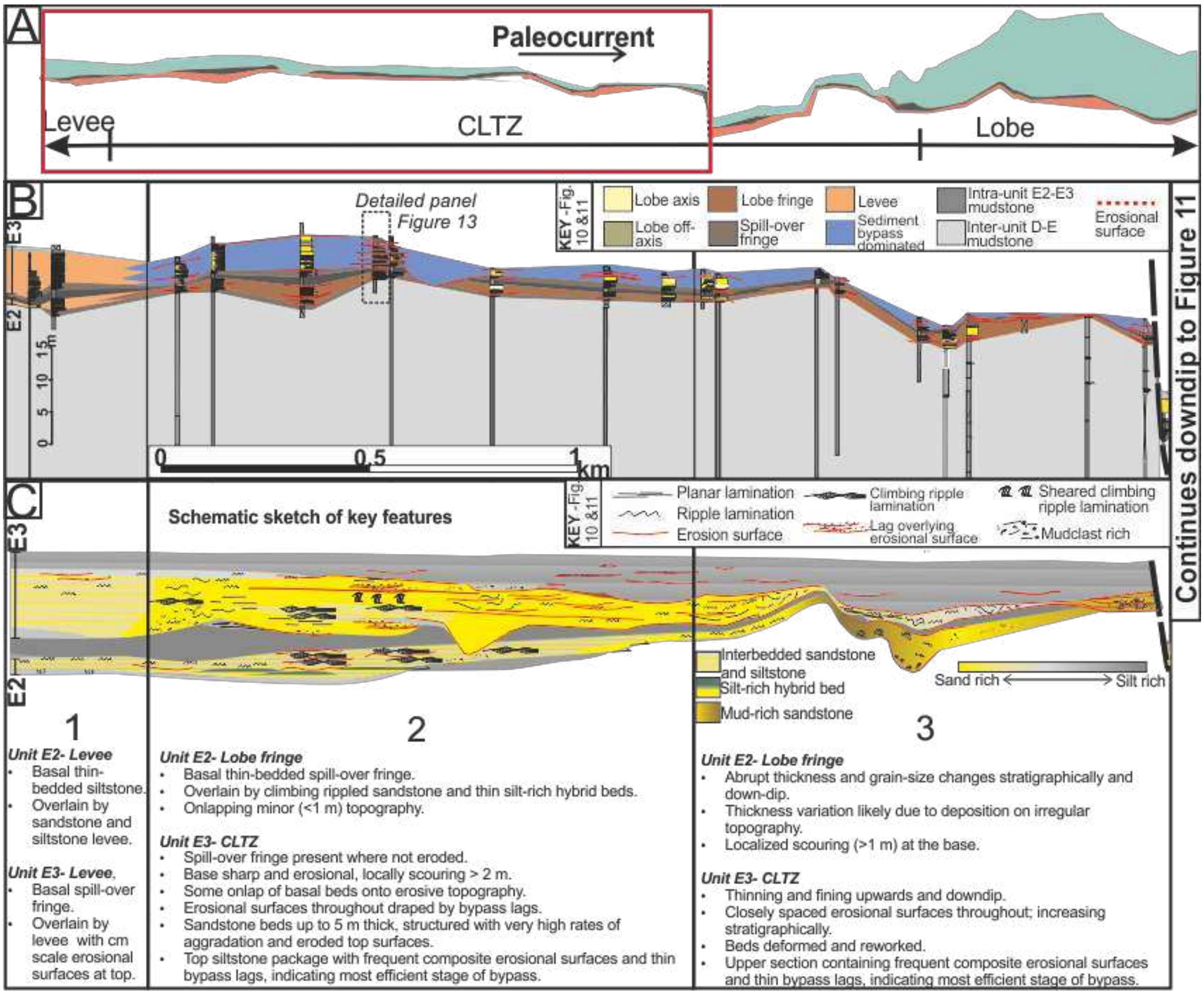
A
Paleocurrent
Levee
CLTZ
Lobe
B
Detailed panel Figure 13
KEY -Fig. 10 &11
Lobe axis
Lobe off-axis
Lobe fringe
Spill-over fringe
Levee
Sediment bypass dominated
Intra-unit E2-E3 mudstone
Inter-unit D-E mudstone
Erosional surface
E3
E2
0 5 10 15 m
0 0.5 1 km
Continues downdip to Figure 11
C
Schematic sketch of key features
KEY -Fig. 10 &11
Planar lamination
Ripple lamination
Erosion surface
Climbing ripple lamination
Lag overlying erosional surface
Sheared climbing ripple lamination
Mudclast rich
Interbedded sandstone and siltstone
Silt-rich hybrid bed
Mud-rich sandstone
Sand rich
Silt rich
1
Unit E2- Levee
• Basal thin-bedded siltstone.
• Overlain by sandstone and siltstone levee.
Unit E3- Levee,
• Basal spill-over fringe.
• Overlain by levee with cm scale erosional surfaces at top.
2
Unit E2- Lobe fringe
• Basal thin-bedded spill-over fringe.
• Overlain by climbing rippled sandstone and thin silt-rich hybrid beds.
• Onlapping minor (<1 m) topography.
Unit E3- CLTZ
• Spill-over fringe present where not eroded.
• Base sharp and erosional, locally scouring > 2 m.
• Some onlap of basal beds onto erosive topography.
• Erosional surfaces throughout draped by bypass lags.
• Sandstone beds up to 5 m thick, structured with very high rates of aggradation and eroded top surfaces.
• Top siltstone package with frequent composite erosional surfaces and thin bypass lags, indicating most efficient stage of bypass.
3
Unit E2- Lobe fringe
• Abrupt thickness and grain-size changes stratigraphically and down-dip.
• Thickness variation likely due to deposition on irregular topography.
• Localized scouring (>1 m) at the base.
Unit E3- CLTZ
• Thinning and fining upwards and downdip.
• Closely spaced erosional surfaces throughout; increasing stratigraphically.
• Beds deformed and reworked.
• Upper section containing frequent composite erosional surfaces and thin bypass lags, indicating most efficient stage of bypass.

1278

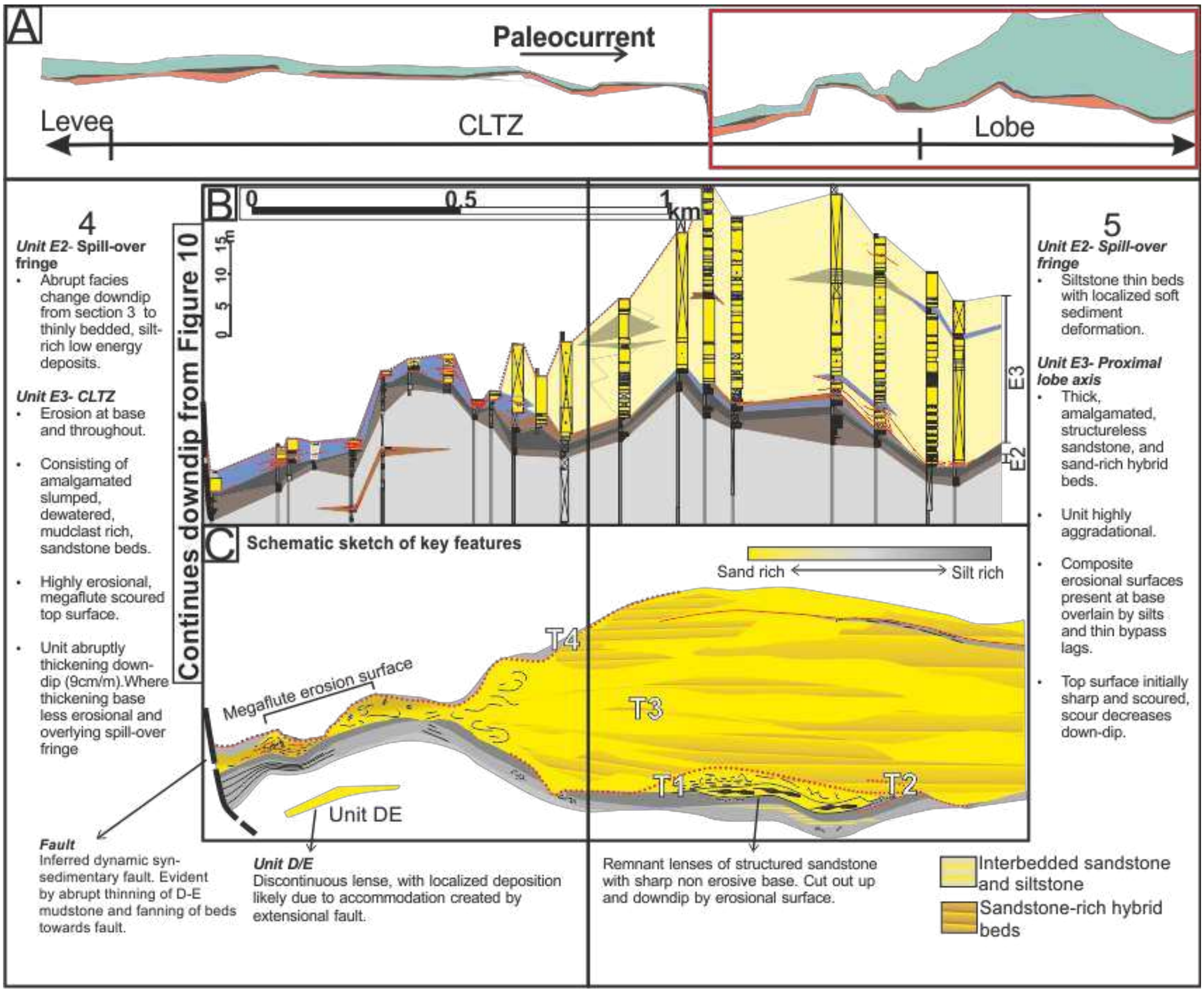

A
Paleocurrent
Levee
CLTZ
Lobe
B
0
0.5
1 km
0 5 10 15 m
Continues downdip from Figure 10
E3
E2
C
Schematic sketch of key features
Sand rich
Silt rich
T4
T3
T1
T2
Megaflute erosion surface
Unit DE
4
Unit E2- Spill-over fringe
• Abrupt facies change downdip from section 3 to thinly bedded, silt-rich low energy deposits.
Unit E3- CLTZ
• Erosion at base and throughout.
• Consisting of amalgamated slumped, dewatered, mudclast rich, sandstone beds.
• Highly erosional, megaflute scoured top surface.
• Unit abruptly thickening down-dip (9cm/m).Where thickening base less erosional and overlying spill-over fringe
5
Unit E2- Spill-over fringe
• Siltstone thin beds with localized soft sediment deformation.
Unit E3- Proximal lobe axis
• Thick, amalgamated, structureless sandstone, and sand-rich hybrid beds.
• Unit highly aggradational.
• Composite erosional surfaces present at base overlain by silts and thin bypass lags.
• Top surface initially sharp and scoured, scour decreases down-dip.
Fault
Inferred dynamic syn-sedimentary fault. Evident by abrupt thinning of D-E mudstone and fanning of beds towards fault.
Unit D/E
Discontinuous lense, with localized deposition likely due to accommodation created by extensional fault.
Remnant lenses of structured sandstone with sharp non erosive base. Cut out up and downdip by erosional surface.
Interbedded sandstone and siltstone
Sandstone-rich hybrid beds

1279

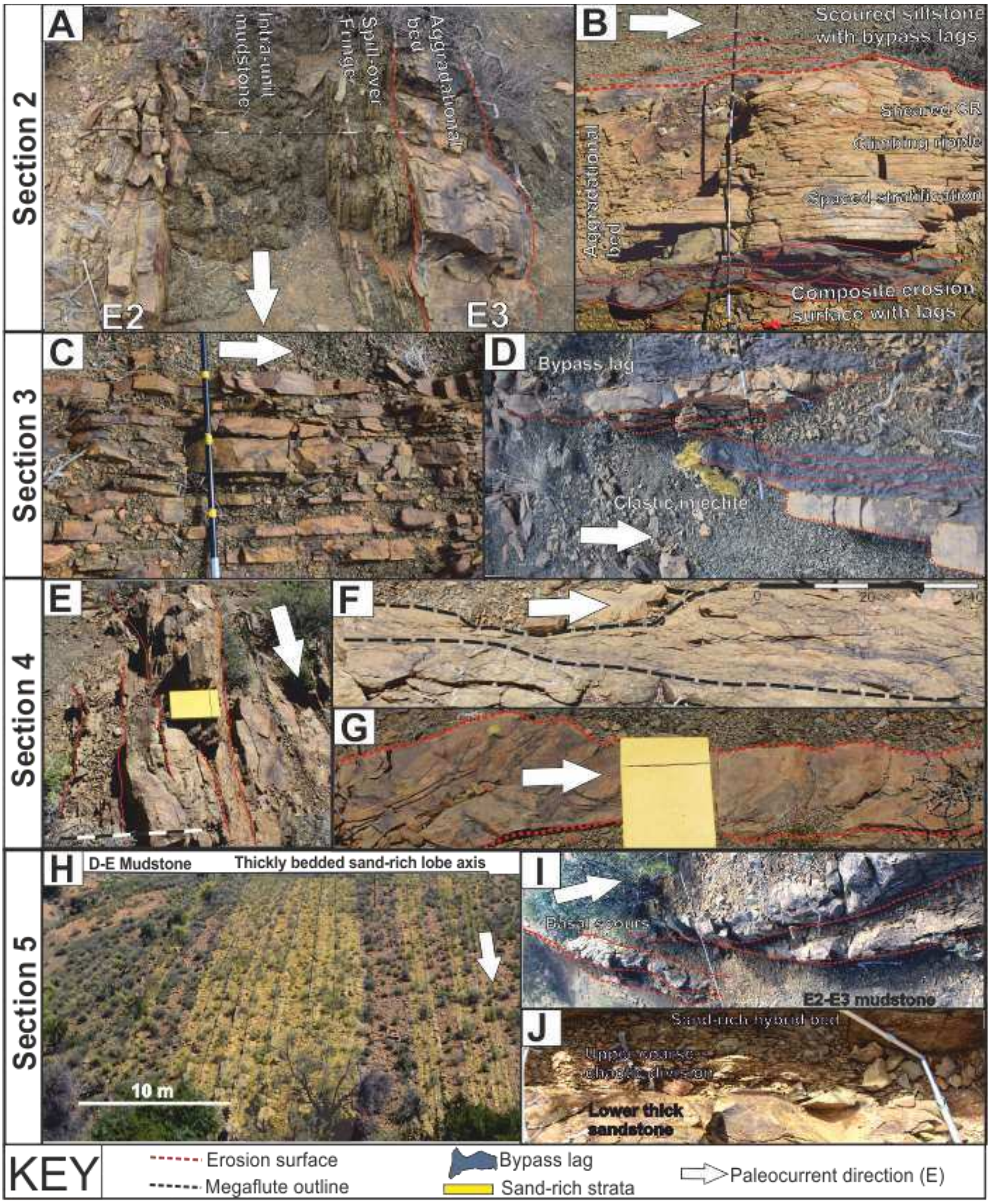

Section 2
A
Intra-unit mudstone
Spill-over Fringe
Aggradational bed
E2
E3
B
Scoured siltstone with bypass lags
Sheared CR
Climbing ripple
Spaced stratification
Aggradational bed
Composite erosion surface with lags
Section 3
C
D
Bypass lag
Clastic injectite
Section 4
E
F
G
Section 5
H
D-E Mudstone
Thickly bedded sand-rich lobe axis
10 m
I
Basal scours
E2-E3 mudstone
J
Sand-rich hybrid bed
Lower thick sandstone
KEY
Erosion surface
Megaflute outline
Bypass lag
Sand-rich strata
Paleocurrent direction (E)

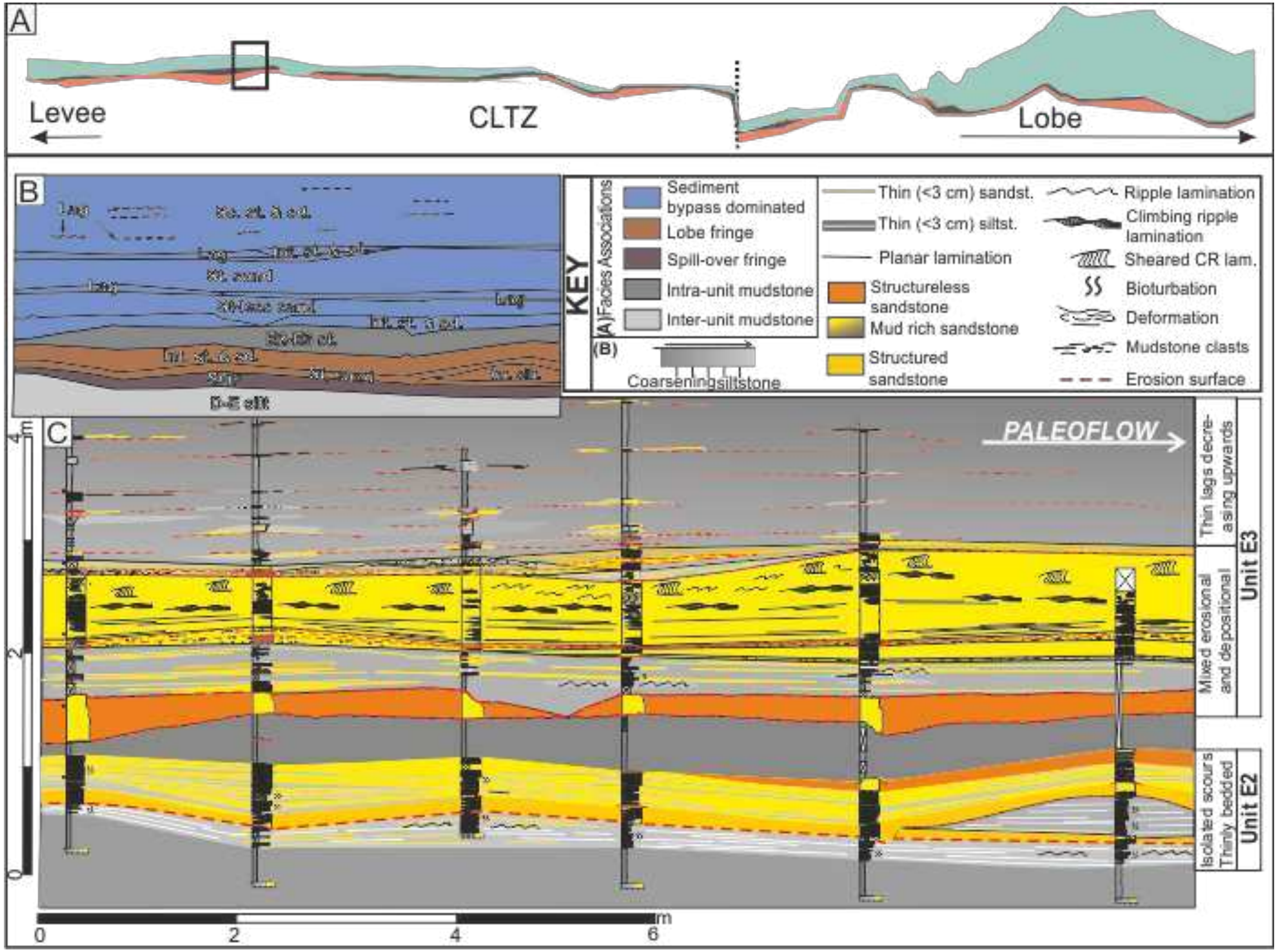

A
Levee
CLTZ
Lobe
B
C
KEY
(A) Facies Associations
Sediment bypass dominated
Lobe fringe
Spill-over fringe
Intra-unit mudstone
Inter-unit mudstone
(B)
Coarsening siltstone
Thin (<3 cm) sandst.
Thin (<3 cm) siltst.
Planar lamination
Structureless sandstone
Mud rich sandstone
Structured sandstone
Ripple lamination
Climbing ripple lamination
Sheared CR lam.
Bioturbation
Deformation
Mudstone clasts
Erosion surface
PALEOFLOW
Thin lags decreasing upwards
Mixed erosional and depositional
Unit E3
Isolated scours
Thinly bedded
Unit E2
0
2
4
6
m

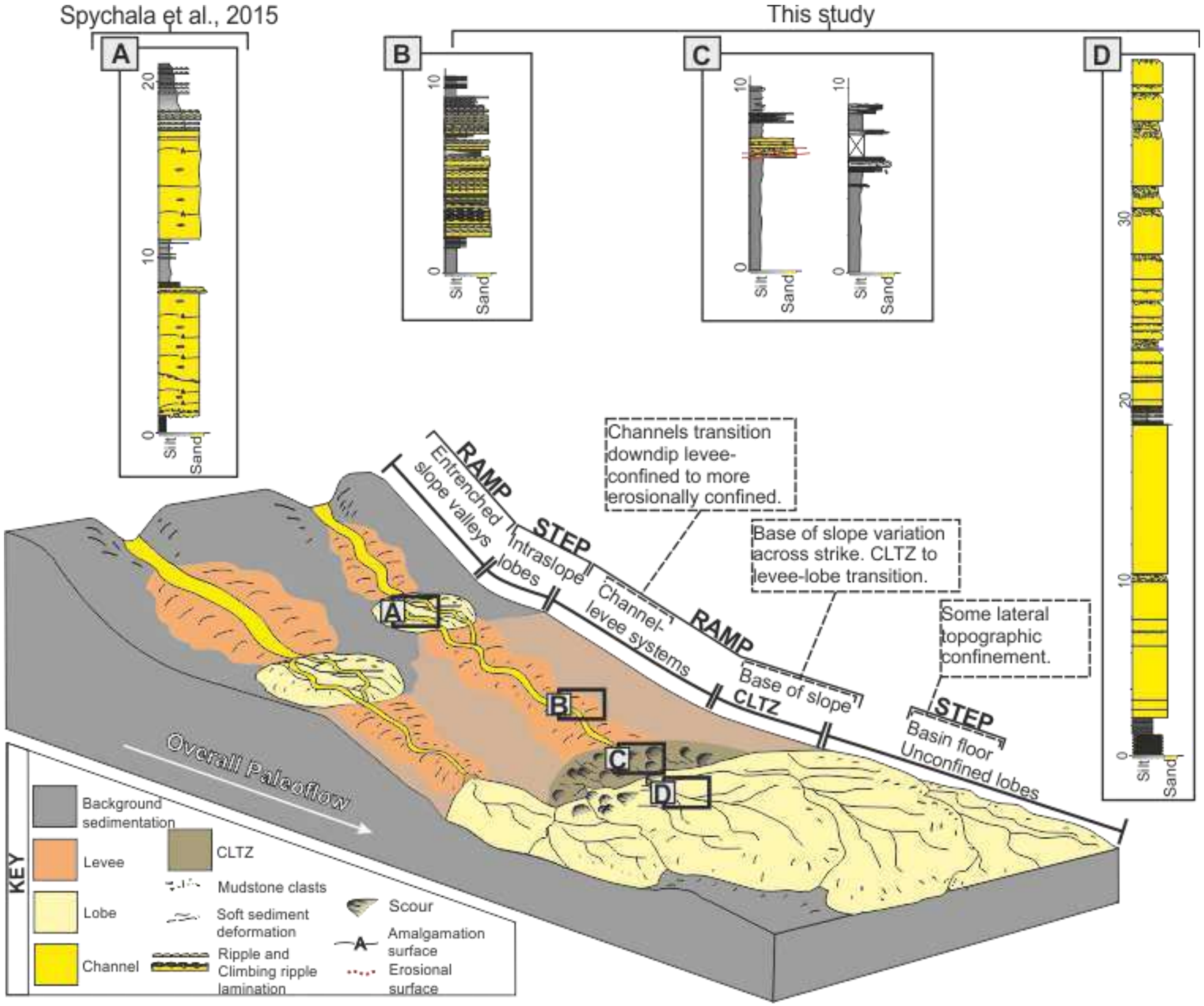

Spychala et al., 2015
This study
A
B
C
D
Silt
Sand
RAMP
Entrenched slope valleys
STEP
Intraslope lobes
Channel-levee systems
RAMP
Base of slope
CLTZ
STEP
Basin floor
Unconfined lobes
Channels transition downdip levee-confined to more erosionally confined.
Base of slope variation across strike. CLTZ to levee-lobe transition.
Some lateral topographic confinement.
Overall Paleoflow
KEY
Background sedimentation
Levee
Lobe
Channel
CLTZ
Mudstone clasts
Soft sediment deformation
Ripple and Climbing ripple lamination
Scour
Amalgamation surface
Erosional surface

1282

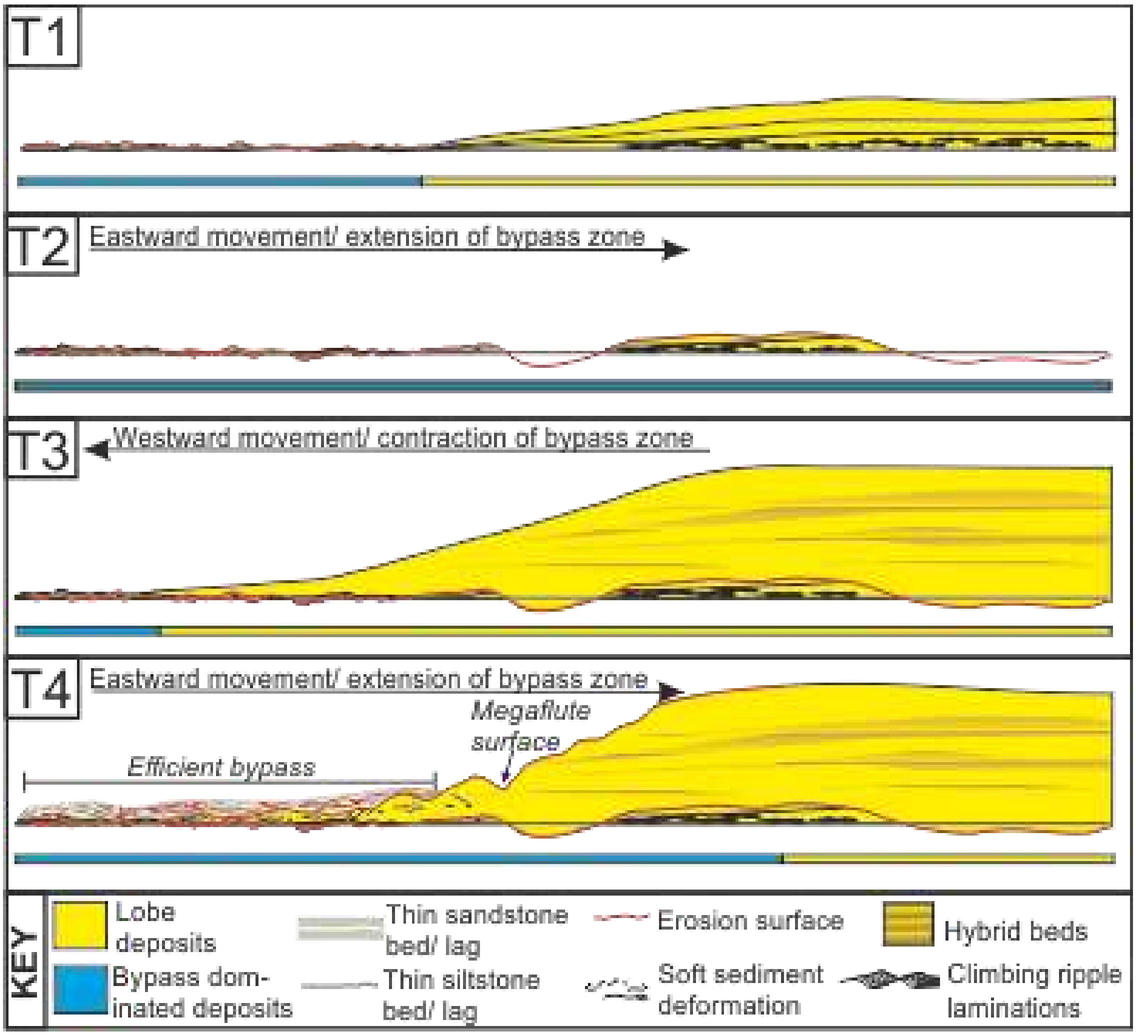

T1
T2
Eastward movement/ extension of bypass zone
T3
Westward movement/ contraction of bypass zone
T4
Eastward movement/ extension of bypass zone
Megaflute surface
Efficient bypass
KEY
Lobe deposits
Bypass dom- inated deposits
Thin sandstone bed/ lag
Thin siltstone bed/ lag
Erosion surface
Soft sediment deformation
Hybrid beds
Climbing ripple laminations

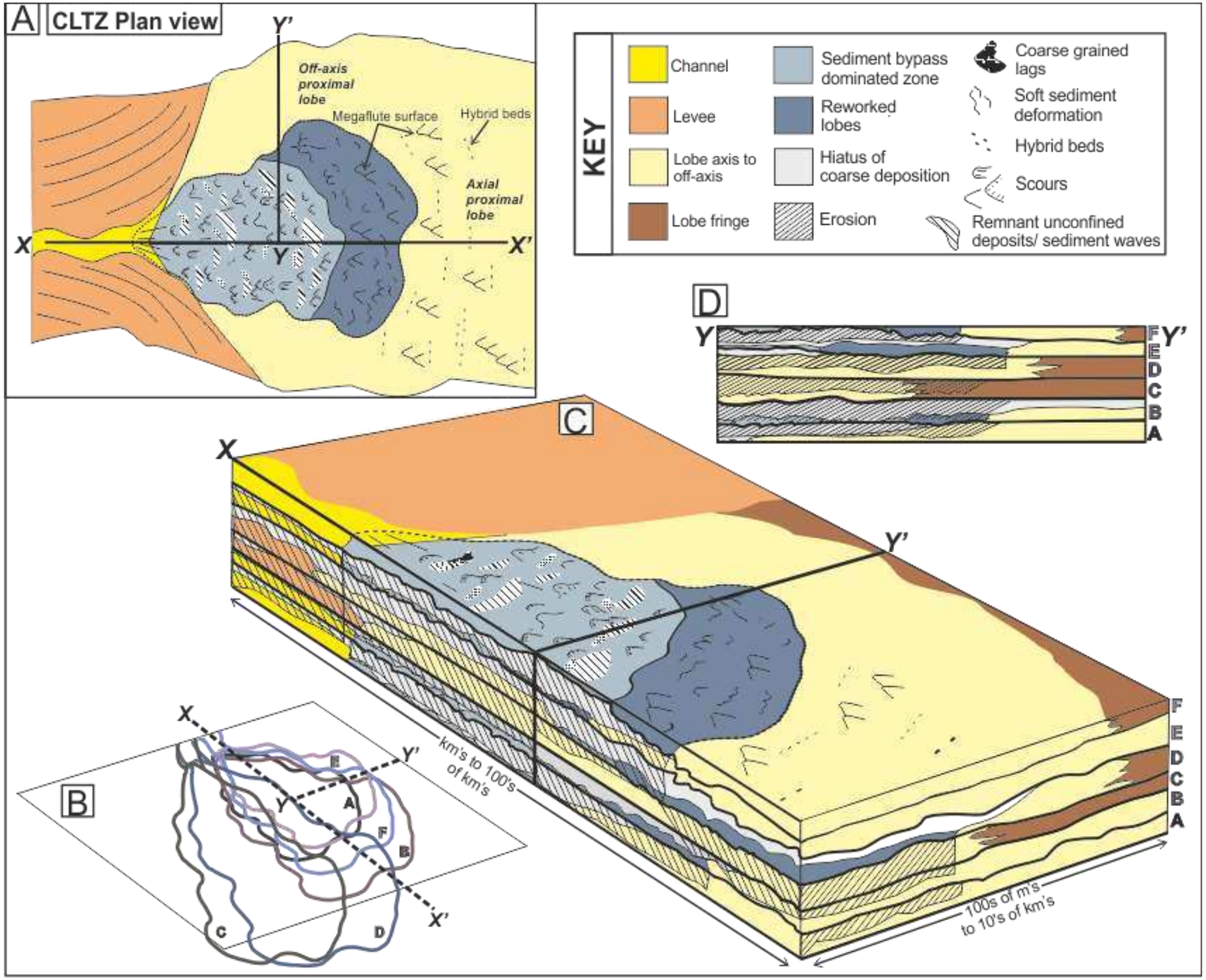

A
CLTZ Plan view
Y'
Off-axis proximal lobe
Megaflute surface
Hybrid beds
Axial proximal lobe
X
Y
X'
KEY
Channel
Levee
Lobe axis to off-axis
Lobe fringe
Sediment bypass dominated zone
Reworked lobes
Hiatus of coarse deposition
Erosion
Coarse grained lags
Soft sediment deformation
Hybrid beds
Scours
Remnant unconfined deposits/ sediment waves
D
Y
Y'
F
E
D
C
B
A
C
X
Y'
km's to 100's of km's
100s of m's to 10's of km's
B
X
Y'
Y
X'

1284 *Table 1*

Facies	Lithology and sedimentary structures	Bed and package thickness and geometry	Interpretation	Architectural element
Amalgamated structureless sandstone (Fig. 5A)	Fine-grained sandstone, commonly amalgamated. Weak-normal grading at bed tops. Erosional bases and rare flutes and grooves. Dewatering structures (e.g. pipes) and deformation structures (e.g. ball and pillow structures) at bed contacts. Rare, discontinuous mudstone clast layers (clasts <3 cm a-axis, sub-angular and elongate, <5% volume) dispersed within beds and present at amalgamation surfaces.	Beds 0.1-1 m thick. Packages up to 30 m thick. Beds and packages tabular.	Structureless and weak normal grading suggests deposition from sand-rich high-density turbidity currents (Bouma, 1962; Lowe, 1982; Mutti, 1992; Kneller and Branney, 1995). Lack of structures indicates rapid deposition. Dispersed rip-up clasts and clast-rich amalgamated contacts suggest progressive aggradation from depletive steady high-density flow (Kneller and Branney, 1995). Dewatering structures form post-deposition, due to sediment liquefaction (Mulder and Alexander, 2001; Stow and Johansson, 2002).	Lobe axis
Structured sandstone (Fig. 5B)	Fine-grained sandstone with planar, current ripple and climbing ripple lamination; dewatering structures (e.g. pipes) and deformation structures (e.g. ball and pillow structures). Climbing ripple lamination can exhibit a high angle of climb (15-30°) and stoss-side preservation of laminae. Sheared and overturned climbing ripple laminations present in localized areas at bed tops.	Beds 0.05-1m thick. Packages up to 5 m thick. Beds and packages tabular to lenticular	Planar lamination indicate upper stage plane bed conditions (Allen, 1984; Talling et al., 2012); or traction carpet deposition (spaced stratification) (Hiscott and Middleton, 1980; Lowe, 1982; Sumner et al., 2008; Cartigny et al., 2013). High angle climbing ripples form from continuous bedload traction under high aggradation rates (Allen, 1970; Jobe et al., 2012; Morris et al., 2014). Sheared and overturned climbing ripple laminations, are soft-sediment deformation structures (Allen and Banks, 1972; Allen, 1985).	Lobe axis Lobe off-axis External levee
Lenticular mudstone clast conglomerate and sandstones (Fig. 5C)	Poorly sorted fine- and medium- grained sandstone and siltstone with well- to sub-round mudstone clasts (mm up to 15 cm, a-axis). Beds can be matrix- or clast-supported comprising 10-80% clasts by volume. Commonly, overlies erosion surfaces at the bases of sandstone packages or interstratified with siltstone.	Beds 0.5-1.5 m packages up to 2 m thick. Beds and packages often lenticular with sharp undulating base and top surfaces. Highly discontinuous	Deposition in high energy environment, fluctuating between erosion, bypass and deposition. Accumulation of a residual lag from bypassing energetic sediment gravity flows (Mutti and Normark, 1987; Gardner et al., 2003; Beaubouef, 2004; Brunt et al., 2013b; Stevenson et al., 2015). Intraformational mudstone clasts collect in areas of reduced bed shear stress including scours or	Sediment bypass-dominated zone

			downdip of gradient change induced hydraulic jumps (Johnson et al., 2001).	
Scoured siltstone and sandstone (Fig. 5D)	Thin-bedded siltstone with thin, lenticular and poorly sorted silty sandstone beds; both overlie and are cut by erosion surfaces. Several erosion surfaces can coalesce to form composite surfaces. Scour dimensions are typically <3-15 m long, 1-3 m wide and <1 m deep, locally displaying asymmetry with steeper headwalls, in planform exposures.	Beds and packages 0.02-1 m thick. Lenticular, sharp and undulating bases and tops. Highly discontinuous.	Multiple isolated and composite scour surfaces indicate protracted periods of erosion and sediment bypass downdip (Beaubouef et al., 1999; Chapin et al., 1994; Kane et al., 2009b; Macdonald et al., 2011a, 2011b; Macauley and Hubbard, 2013; Hofstra et al., 2015; Stevenson et al., 2015). Megaflutes interpreted from planform scour geometries.	Sediment bypass-dominated zone
Hybrid beds (Fig. 5E)	Bipartite bed. Lower division comprising weakly normally graded fine-grained sandstone, dewatering structures, rare planar lamination, and mudstone clast layers (clasts 1- 10 cm a-axis, sub-angular, elongated, <5% volume). Upper division comprising poorly sorted silt sandstone with dispersed mudstone clasts (mm-cm scale, sub-angular, elongate, >50% volume) and plant fragments. Two types: i) thick sand-rich lower division with rare mudstone clast layers, poorly sorted, coarse-grained upper division; or ii) thin silty lower division, poorly sorted upper division, with a minor coarse-grained component.	Beds 0.2-2 m thick. i) Lower division 0.2-1 m thick. Upper division 0.05-0.5 m thick. ii) Lower division <0.2 m thick. Upper division 0.05-0.5 m thick. Beds generally tabular. Packages up to 20 m thick and generally tabular.	Deposition of the lower division from a sand-rich turbidity current with the 'linked' poorly sorted upper division. Hybrid event beds (Haughton et al., 2003, 2009) form preferentially towards the base and fringes of lobe deposits (e.g. Hodgson, 2009; Talling, 2013), but can form in any environment where mud and mudstone clasts are entrained into the turbulent flow, increasing sediment volume, damping turbulence, and developing high-concentration to pseudo-laminar flow conditions (e.g. Ito, 2008; Haughton et al., 2003, 2009; Baas et al., 2011).	Lobe axis Lobe off-axis Lobe fringe
Interbedded sandstone and siltstone (Fig. 5F)	Three types documented based on bed thickness and sandstone proportion: i) interbedded siltstone and very fine-grained sandstone. Current, and low angle (<5°) climbing, ripple laminated. 'Pinch and swell' bed geometry common in cross-section where ripple sets are draped by siltstone;	i) Beds 2-30 cm thick, packages 0.5-6 m thick. Beds tabular or show thickness change with ripple geometries. ii) Beds mm-20 cm thick, packages 0.5-7 m thick.	Deposition from dilute turbidity currents, with the finer sediment residual within the flow after deposition of the coarser fraction of sediment load. Climbing ripples form through late stage tractional modification of waning or low-density flows, with high sediment fall out rates (Lowe, 1988). Thin beds and low angle of climb suggests lower rates of suspended load fallout. Starved	Lobe off-axis Lobe fringe Spill-over fringe External levee

	ii) thin-bedded siltstone with minor sandstone beds and silt rich hybrid beds. Ripples are 1-2 cm in height and <4 cm wavelength; iii) Thin (<2 cm) siltstone beds with rare normally graded very fine-grained sandstone at bed bases. Bioturbation fabric (*Planolites*) is common throughout (ii) and (iii).	Beds and packages tabular. iii) mm-5 cm thick. Packages 0.1-3 m thick and laterally extensive for 10's kms.	ripples indicate deposition from sediment-limited weak traction currents (Jobe et al., 2012). Very thin-bedded, laterally extensive, silt-dominated deposits are interpreted as derived from numerous dilute turbidity currents.	
Contorted and chaotic deposits (Fig. 5G)	Sandstone and siltstone, coherently folded to highly disaggregated. Contorted clasts supported by a poorly sorted silt-prone matrix. Chaotic deposits have a poorly sorted matrix of very fine-grained sandstone to coarse-grained siltstone beds, lack internal structure and contain dispersed sub-angular, elongate, mm-cm scale mudstone clasts and plant fragments.	Beds cms-2 m thick. Packages up to 10 m thick, extending laterally for 10's of meters.	These facies are interpreted as mass flow deposits derived from remobilization processes to form slides and slumps. Highly disaggregated examples are interpreted as debrites.	Not characteristic of any specific environment, can occur in association with all architectural elements.
Hemipelagic mudstone (Fig. 5H)	Claystone and fine-grained siltstone, with mm scale laminations or structureless.	Beds mm-3 cm. Packages up to 70 m thick. Packages highly regionally extensive for 10's of kms up-dip, down-dip and laterally.	Background hemipelagic deposition, with occasional distal dilute turbidity currents. Regional drapes during shutdown of sand and coarse coarse-grained silt supply.	Regional mudstone

Table 2

Location	CLTZ Length (km)	Basin/Fan Area (km²)	Reference
Agadir Channel mouth	30-60	>40,000	Wynn et al. (2002a)
Umnak Channel mouth	100–120	48,000	Kenyon and Millington (1995)
Lisbon Canyon mouth	40	25,000	Wynn et al. (2002a)
Rhone Fan	30-40	>60,000	Wynn et al. (2002a) Kenyon et al. (1995)
Valencia Fan	>100	>10,000	Morris et al. (1998) Palanques et al. (1995)
Navy Fan	3-4	560	Normark et al. (1979)
Unit E, Fort Brown Fm. Karoo basin	6	680	This study

Table 3

Characteristic	Description	Further examples
Thin stratigraphic expression	Entire thickness varies from a surface separating lobes from channel-levee to a <5 m stratigraphic expression.	Mutti and Normark, 1987; Gardner et al., 2003; van der Merwe et al., 2014; Pyles et al., 2014
Amalgamated erosional features	Intense vertical concentration of erosive surfaces, both sub-horizontal, and as discrete scour forms, including megaflutes	Mutti and Normark, 1987; Wynn et al., 2002a; Macdonald et al., 2011a; Ito et al., 2014; Hofstra et al., 2015; Pemberton et al., 2016
Coarse grained lag deposits	Mudclast horizons and relatively coarse-grained sediment (equating to medium sand in the Fort Brown Fm.) overlying erosive surfaces	Mutti and Normark, 1987; Wynn et al., 2002a; Ito et al., 2014; Stevenson et al., 2015
Aggradational bedforms, including sediment waves	Abundance of structureless sandstone, spaced stratification, climbing ripple and sheared ripple laminations in the Karoo suggesting rapid deposition. Elsewhere cross stratified gravels	Mutti and Normark, 1987; Vincente Bravo and Robles, 1995; Morris et al., 1998; Wynn et al., 2002b; Ito et al., 2014
Soft-sediment deformation	Small scale localized slumping and overturned bedding reflecting rapid deposition	Mutti and Normark, 1987; Wynn et al., 2002a
Thin bedded siltstone packages	Preservation of thin-bedded siltstones representing low-energy flows demonstrate that aggradation was sufficiently rapid to preserve fine-grained deposits	-
Interfingering with downdip proximal lobes	Reflecting rapid migration of the CLTZ system in response to controls external to the CLTZ	Gardner et al., 2003
Interfingering with updip and lateral levee deposits	Reflecting growth and decay of CLTZ and migration of feeder systems	-
Sand-rich hybrid beds within proximal lobes	Significant erosion causes evolution of flows over CLTZ	-